

Scalable Computations for Generalized Mixed Effects Models with Crossed Random Effects Using Krylov Subspace Methods

Pascal Kündig^{*†§}

Fabio Sigrist^{†*}

June 11, 2025

Abstract

Mixed effects models are widely used for modeling data with hierarchically grouped structures and high-cardinality categorical predictor variables. However, for high-dimensional crossed random effects, current standard computations relying on Cholesky decompositions can become prohibitively slow. In this work, we present novel Krylov subspace-based methods that address several existing computational bottlenecks. Among other things, we theoretically analyze and empirically evaluate various preconditioners for the conjugate gradient and stochastic Lanczos quadrature methods, derive new convergence results, and develop computationally efficient methods for calculating predictive variances. Extensive experiments using simulated and real-world data sets show that our proposed methods scale much better than Cholesky-based computations, for instance, achieving a runtime reduction of approximately two orders of magnitudes for both estimation and prediction. Moreover, our software implementation is up to 10'000 times faster and more stable than state-of-the-art implementations such as `lme4` and `glmmTMB` when using default settings. Our methods are implemented in the free C++ software library `GPBoost` with high-level Python and R packages.

1 Introduction

Mixed effects models are widely used in various scientific disciplines for modeling data with hierarchically grouped structures [Laird and Ware, 1982, Pinheiro and Bates, 2000]. High-dimensional crossed random effects occur frequently in practice, e.g., when modeling ratings in recommender systems with categorical grouping variables corresponding to customers and products [Gao and Owen, 2017, Ghosh et al., 2022a, Simchoni and Rosset, 2023] or, in general, when there are high-cardinality categorical predictor variables [Simchoni and Rosset, 2021, Sigrist, 2023b]. However, current standard Cholesky decomposition-based computations can become prohibitively slow for high-dimensional crossed random effects. For instance, the cost of computing Cholesky factors of sparse matrices can be of cubic complexity in the dimension of the random effects [Pandolfi et al., 2024].

Various methods have been proposed to overcome this computational bottleneck, including method of moments estimation [Gao and Owen, 2017, 2020], collapsed Gibbs samplers [Papaspiliopoulos et al., 2020, 2023], backfitting algorithms [Ghosh et al., 2022b,a], composite likelihoods [Bellio et al., 2023, Xu et al., 2023], and variational inference [Xu et al., 2023, Goplerud et al., 2025]. Furthermore, the preconditioned conjugate gradient (CG) method [Saad, 2003] with relatively simple diagonal or block-diagonal preconditioners has been applied to solve high-dimensional mixed model equations [Strandén and Lidauer, 1999, 2001, Tsuruta et al., 2001, Taskinen et al., 2017, Garrick et al., 2019, Vandenplas et al., 2018]. Recently, Pandolfi et al. [2024] have used the CG method in Gibbs sampling for Bayesian generalized linear mixed models (GLMMs). For Gaussian likelihoods and the special case where all random effects have the same variance, Border and Becker [2019] and Cheng et al. [2023] use stochastic Lanczos quadrature (SLQ) [Ubaru et al., 2017] without preconditioning in combination with a shift-invariance property to calculate log-determinants in log-likelihoods. However, without

^{*}Lucerne University of Applied Sciences and Arts

[†]Seminar for Statistics, ETH Zurich

[‡]University of Basel

[§]Corresponding author: pascal.kuendig@gmail.com

preconditioning, SLQ-approximated log-determinants have high variance and are thus inaccurate; see our theoretical and empirical analyses below. Overall, there are two major unsolved computational challenges: (i) efficiently computing log-determinants in log-likelihoods and their gradients, and (ii) solving high-dimensional sparse linear systems with many right-hand sides for prediction.

In this article, we show how Krylov subspace methods, such as the preconditioned CG and SLQ methods, can be used for computationally efficient parameter estimation and the calculation of posterior predictive distributions for generalized mixed effects models (GMMs), a term we use to denote mixed effects models with linear and non-linear fixed effects functions and general response variable distributions. For non-Gaussian likelihoods, marginal likelihoods are approximated using the Laplace approximation since it is computationally efficient and converges asymptotically to the correct quantity. Supporting this argument, we show in Figure 1 the estimated variance parameter of one random effect in a model with two crossed random effects obtained with a Laplace approximation for varying numbers of repeated observations d per random effect realization on simulated data with a Bernoulli likelihood and the setting described in Section 5.1 with $m = 4'000$. Estimation is done using the Krylov subspace methods introduced in this paper and repeated on 100 simulated data sets for every d . Figure 1 shows that the variance parameter estimator has a small downward bias which vanishes as d grows.

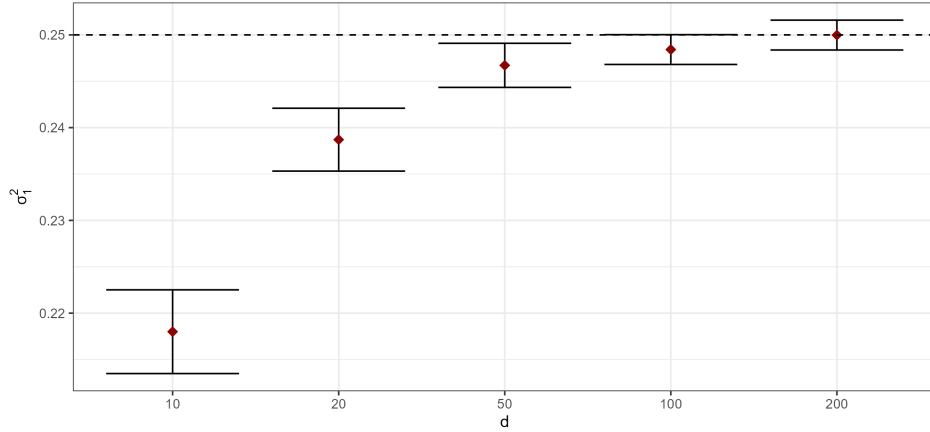


Figure 1: Estimated variance parameter σ_1^2 obtained with a Laplace approximation vs. different numbers of repeated observations d per random effect realization for binary data. The red rhombi represent means and the whiskers are $\pm 2 \times$ standard errors. The dashed line indicates the true parameter $\sigma_1^2 = 0.25$.

Krylov subspace methods allow for fast computations as they rely on matrix-vector multiplications with sparse matrices which can be trivially parallelized. We use the preconditioned CG and SLQ methods to solve sparse linear systems and to calculate log-determinants in log-likelihoods, respectively. Gradients of log-marginal likelihoods are calculated using stochastic trace estimation (STE) with almost no computational overhead once likelihoods are evaluated. We theoretically and empirically analyze several preconditioners with regard to the accuracy of SLQ approximations and the CG method’s convergence speed. Our theoretical results show that approximations with the SLQ method are expected to be accurate and that the CG method converges rapidly. In addition, we provide theoretical and empirical results showing that the symmetric successive over-relaxation (SSOR) preconditioner is superior compared to the popular diagonal preconditioner for both the CG and the SLQ methods. Furthermore, we introduce efficient and accurate simulation-based methods for calculating predictive variances when the number of prediction points is large. In experiments with simulated and real-world data, we obtain a reduction in runtime of approximately two orders of magnitude compared to Cholesky-based computations for estimation and prediction while having essentially identical accuracy. Moreover, our software implementation in the **GPBoost** library is up to 10’000 times faster and more stable than the state-of-the-art **lme4** and **glmmTMB** packages when using default settings.

2 Preliminaries on Generalized Mixed Effects Models

We assume that the response variable $y = (y_1, \dots, y_n)^T \in \mathbb{R}^n$ follows a distribution with a density $p(y|\mu, \xi) = \prod_{i=1}^n p(y_i|\mu_i, \xi)$, where $\mu \in \mathbb{R}^n$ are, potentially link function-transformed, parameters, and $\xi \in \Xi \subset \mathbb{R}^r$ are auxiliary parameters. For instance, μ_i and ξ can be the mean and variance of a Gaussian distribution, the log-mean and the shape parameter of a gamma likelihood, or μ_i can be the logit-transformed success probability of a Bernoulli distribution for which there is no additional parameter ξ . The main parameters of interest μ are modeled as the sum of fixed $F(X)$ and random effects Zb :

$$\mu = F(X) + Zb, \quad b \sim N(0, \Sigma),$$

where $X \in \mathbb{R}^{n \times p}$ contains predictor variables. In generalized linear mixed effects models (GLMMs), the fixed effects function is linear, $F(X) = X\beta$, but $F(\cdot)$ can also be modeled using machine learning methods such as regression trees [Hajjem et al., 2011, Sela and Simonoff, 2012, Fu and Simonoff, 2015], random forests [Hajjem et al., 2014], tree-boosting [Sigrist, 2022, 2023a], or deep neural networks [Simchoni and Rosset, 2021, 2023, Avanzi et al., 2024]. The latent Gaussian variables $b = (b_1^T, b_2^T, \dots, b_K^T)^T \in \mathbb{R}^m$ consist of K grouped random effects $b_j \in \mathbb{R}^{m_j}$, $j \in \{1, \dots, K\}$, $m = \sum_{j=1}^K m_j$, and the covariance matrix $\Sigma \in \mathbb{R}^{m \times m}$ is diagonal and depends on a set of variance parameters $\theta = \{\sigma_1^2, \sigma_2^2, \dots, \sigma_K^2\}$:

$$\Sigma = \text{diag}(\underbrace{\sigma_1^2, \dots, \sigma_1^2}_{m_1\text{-times}}, \underbrace{\sigma_2^2, \dots, \sigma_2^2}_{m_2\text{-times}}, \dots, \underbrace{\sigma_K^2, \dots, \sigma_K^2}_{m_K\text{-times}}) \in \mathbb{R}^{m \times m}.$$

In addition, $Z = (Z_1, Z_2, \dots, Z_K) \in \mathbb{R}^{n \times m}$, $Z_j \in \mathbb{R}^{n \times m_j}$, is usually a binary incidence matrix that maps the random effects to the corresponding observations, but it can also contain predictor variables when modeling random coefficients. We denote such a model as a generalized mixed effects model (GMM). Since we use the Laplace approximation, we further assume that $p(y|\mu, \xi)$ is log-concave in μ .

2.1 Parameter estimation

For parameter estimation, the marginal likelihood $p(y|F, \theta, \xi) = \int p(y|\mu, \xi)p(b|\theta)db$ is typically maximized. However, for non-Gaussian likelihoods, there is usually no analytic expression for this marginal likelihood and an approximation has to be used. We choose the Laplace approximation since it is computationally efficient and converges asymptotically to the correct quantity. A Laplace approximation to the negative log-marginal likelihood $-\log(p(y|F, \theta, \xi))$ modulo constant terms is given by

$$L^{LA}(y|F, \theta, \xi) = -\log p(y|\mu^*, \xi) + \frac{1}{2}b^{*T}\Sigma^{-1}b^* + \frac{1}{2}\log \det(\Sigma) + \frac{1}{2}\log \det(\Sigma^{-1} + Z^TWZ), \quad (1)$$

where $\mu^* = F(X) + Zb^*$, $b^* = \arg\max_b \log p(y|\mu, \xi) - \frac{1}{2}b^T\Sigma^{-1}b$ is the mode of $p(y|\mu, \xi)p(b|\theta)$, and $W \in \mathbb{R}^{n \times n}$ is diagonal with $W_{ii} = -\frac{\partial^2 \log p(y_i|\mu_i, \xi)}{\partial \mu_i^2} \Big|_{\mu=\mu^*}$. The mode b^* is typically found with Newton's method [Williams and Rasmussen, 2006], and one iteration is given by

$$b^{*t+1} = b^{*t} + (Z^TWZ + \Sigma^{-1})^{-1} \left(Z^T \frac{\partial \log p(y|\mu^{*t}, \xi)}{\partial b} - \Sigma^{-1}b^{*t} \right), \quad t = 0, 1, \dots \quad (2)$$

If a first- or second-order optimization method is used for minimizing $L^{LA}(y|F, \theta, \xi)$, gradients with respect to θ , F , and ξ are needed. These gradients can be found, e.g., in Sigrist [2023a]. Note that gradients with respect to F are used, for instance, for GLMMs since $\frac{\partial L^{LA}(y|F, \theta, \xi)}{\partial \beta} = X^T \frac{\partial L^{LA}(y|F, \theta, \xi)}{\partial F}$ when $F(X) = X\beta$.

For Gaussian likelihoods, we can write

$$y = F(X) + Zb + \epsilon, \quad \epsilon \sim N(0, W^{-1}), \quad W = \frac{1}{\sigma^2}I_n,$$

where σ^2 is the error variance and $I_n \in \mathbb{R}^{n \times n}$ an identity matrix. In this case, the Laplace approximation is exact, and the negative log-marginal likelihood can be equivalently calculated without determining the mode b^* as follows:

$$L(y|F, \theta, \xi) = \frac{n}{2}\log(2\pi) + \frac{1}{2}\log \det(\Psi) + \frac{1}{2}(y - F(X))^T\Psi^{-1}(y - F(X)), \quad \Psi = Z\Sigma Z^T + W^{-1}. \quad (3)$$

Since the dimension of the random effects m is usually smaller than the number of observations n , one uses the Woodbury identity

$$\Psi^{-1} = W - WZ(\Sigma^{-1} + Z^T W Z)^{-1} Z^T W \quad (4)$$

for solving linear systems and the matrix determinant lemma to calculate

$$\log \det(\Psi) = \log \det(\Sigma^{-1} + Z^T W Z) + \log \det(\Sigma) + \log \det(W^{-1}). \quad (5)$$

Gradients, e.g., with respect to the variance parameters are given by

$$\frac{\partial L(y|F, \theta, \xi)}{\partial \theta_k} = \frac{1}{2} \text{tr} \left((\Sigma^{-1} + Z^T W Z)^{-1} \frac{\partial \Sigma^{-1}}{\partial \theta_k} + \Sigma^{-1} \frac{\partial \Sigma}{\partial \theta_k} \right) - \frac{1}{2} (y - F(X))^T \Psi^{-1} \frac{\partial \Psi}{\partial \theta_k} \Psi^{-1} (y - F(X)). \quad (6)$$

The Fisher information $\mathcal{I} \in \mathbb{R}^{K \times K}$ for θ , which can be used for Fisher scoring and for obtaining asymptotic confidence sets, is given by

$$(\mathcal{I})_{kl} = \frac{1}{2} \text{tr} \left(\Psi^{-1} \frac{\partial \Psi}{\partial \theta_k} \Psi^{-1} \frac{\partial \Psi}{\partial \theta_l} \right), \quad 1 \leq k, l \leq K. \quad (7)$$

2.2 Prediction

Consider the goal of making predictions for the latent variables

$$\mu_p = F(X_p) + Z_{po}b + Z_{pp}b_p \in \mathbb{R}^{n_p}, \quad (8)$$

where $X_p \in \mathbb{R}^{n_p \times p}$ is the predictor variable matrix of the predictions, $b_p \in \mathbb{R}^{m_p}$ are new random effects which are not in the training data random effects $b \in \mathbb{R}^m$, the matrix $Z_{po} \in \mathbb{R}^{n_p \times m}$ relates b to μ_p , and the matrix $Z_{pp} \in \mathbb{R}^{n_p \times m_p}$ relates the new random effects b_p to μ_p . We have

$$\begin{pmatrix} b \\ \mu_p \end{pmatrix} = \begin{pmatrix} 0 \\ F(X_p) \end{pmatrix} + \begin{pmatrix} (I_m, 0_{m \times m_p}) \\ (Z_{po}, Z_{pp}) \end{pmatrix} \begin{pmatrix} b \\ b_p \end{pmatrix} \sim \mathcal{N} \left(\begin{pmatrix} 0 \\ F(X_p) \end{pmatrix}, \begin{pmatrix} \Sigma & \Sigma Z_{po}^T \\ Z_{po} \Sigma & Z_{po} \Sigma Z_{po}^T + Z_{pp} \Sigma_p Z_{pp}^T \end{pmatrix} \right), \quad (9)$$

where $(I_m, 0_{m \times m_p}) \in \mathbb{R}^{m \times (m+m_p)}$, $I_m \in \mathbb{R}^{m \times m}$ is an identity matrix, $0_{m \times m_p} \in \mathbb{R}^{m \times m_p}$ is a matrix of zeros, and $\Sigma_p = \text{Cov}(b_p)$. Predictions for μ_p are obtained using the posterior predictive distribution $p(\mu_p|y, \theta, \xi)$ which is given by

$$p(\mu_p|y, \theta, \xi) = \int p(\mu_p|b, \theta) p(b|y, \theta, \xi) db \approx \mathcal{N}(\omega_p, \Omega_p)$$

where

$$\omega_p = F(X_p) + Z_{po}b^*, \quad (10)$$

$$\Omega_p = Z_{po} \Sigma Z_{po}^T + Z_{pp} \Sigma_p Z_{pp}^T - Z_{po} \Sigma Z^T \Psi^{-1} Z \Sigma Z_{po}^T \quad (11)$$

$$= Z_{pp} \Sigma_p Z_{pp}^T + Z_{po} (\Sigma^{-1} + Z^T W Z)^{-1} Z_{po}^T. \quad (12)$$

This can be derived using the fact that a Laplace approximation for $p(y|F, \theta, \xi)$ is equivalent to the approximation $p(b|y, \theta, \xi) \approx \mathcal{N}(b^*, (\Sigma^{-1} + Z^T W Z)^{-1})$ since $p(y|F, \theta, \xi) = p(y|F, b, \xi) p(b|\theta) / p(b|y, \theta, \xi)$, and by applying standard results for conditional distributions of multivariate Gaussian distributions.

For the posterior predictive distribution $p(y_p|y, \theta, \xi)$ of the observable response variables y_p , $y_p|\mu_p \sim p(y_p|\mu_p, \xi)$, the integral

$$p(y_p|y, \theta, \xi) = \int p(y_p|\mu_p, \xi) p(\mu_p|y, \theta, \xi) d\mu_p \quad (13)$$

must be additionally calculated. This is analytically intractable for most likelihoods but can be approximated using numerical integration or by simulating from $p(\mu_p|y, \theta, \xi) \approx \mathcal{N}(\omega_p, \Omega_p)$.

For a Gaussian likelihood, the above predictive distributions are exact and available in closed form. The posterior mean in (10) can be equivalently calculated as

$$\omega_p = F(X_p) + Z_{po} \Sigma Z^T \Psi^{-1} (y - F(X)),$$

and $p(y_p|y, \theta, \xi)$ is obtained from $p(\mu_p|y, \theta, \xi)$ by adding a diagonal matrix with the error variance to Ω_p .

Note that, while the above predictive distributions might be less frequently used in classical statistical applications of GLMMs, they are important, e.g., for mixed effects machine learning models [Sigrist, 2022, Simchoni and Rosset, 2023] for high-cardinality categorical variables when probabilistic predictions are required.

3 Krylov Subspace Methods for Generalized Mixed Effects Models

Parameter estimation and prediction for models with high-dimensional crossed random effects involve several time-consuming operations. Specifically, there are the following bottlenecks all involving operations with the high-dimensional sparse matrix $\Sigma^{-1} + Z^T W Z \in \mathbb{R}^{m \times m}$. First, calculating linear solves $(\Sigma^{-1} + Z^T W Z)u = v$, $v \in \mathbb{R}^m$, (i) for quadratic forms of log-marginal likelihoods in (3) after applying the Woodbury identity given in (4), (ii) in Newton’s method for finding the mode, see (2), (iii) for implicit derivatives of the log-marginal likelihood, see Proposition 2.1 in Sigrist [2023a], and (iv) for predictive variances given in (12). The latter is particularly challenging as the number of prediction points n_p is typically large, and the linear system in (12) thus contains many right-hand sides $Z_{p\cdot}^T$. Note that predictive variances are required not only for predictive distributions, but also for predictive means of non-Gaussian response variables, see (13). Second, calculating log-determinants $\log \det(\Sigma^{-1} + Z^T W Z)$ in (approximate) log-marginal likelihoods $L(y|F, \theta, \xi)$ given in (1) and (5) for non-Gaussian and Gaussian likelihoods, respectively. And third, calculating trace terms such as $\text{tr}((\Sigma^{-1} + Z^T W Z)^{-1} \frac{\partial(\Sigma^{-1} + Z^T W Z)}{\partial \theta_k})$ for the derivatives of log-determinants and $\text{tr}(\Psi^{-1} \frac{\partial \Psi}{\partial \theta_k} \Psi^{-1} \frac{\partial \Psi}{\partial \theta_l})$ for entries of the Fisher information. Traditionally, these operations are performed using a Cholesky decomposition of $\Sigma^{-1} + Z^T W Z$. In the following, we show how these operations can be done using Krylov subspace methods.

For linear solves with the matrix $\Sigma^{-1} + Z^T W Z$, we use the preconditioned conjugate gradient (CG) method, which solves a linear system $(\Sigma^{-1} + Z^T W Z)u = v$ by iteratively doing matrix-vector multiplications with $\Sigma^{-1} + Z^T W Z$. This can be done fast since $\Sigma^{-1} + Z^T W Z$ is sparse, and convergence is often achieved with $l \ll m$ iterations. Thus, linear solves can be calculated in $O(lm)$ time complexity. For completeness, the preconditioned CG algorithm is included in Appendix A.6.

Several techniques have been proposed in the literature to calculate log-determinants of large, symmetric positive definite matrices. Dong et al. [2017] find that stochastic Lanczos quadrature (SLQ) [Ubaru et al., 2017] achieves the highest accuracy and fastest runtime compared to other methods. In this article, we use the SLQ method in combination with the preconditioned CG method to approximate $\log \det(\Sigma^{-1} + Z^T W Z)$. Specifically, we first note that

$$\log \det(\Sigma^{-1} + Z^T W Z) = \log \det(P) + \log \det(P^{-\frac{1}{2}}(\Sigma^{-1} + Z^T W Z)P^{-\frac{T}{2}}), \quad (14)$$

where P is a symmetric positive definite preconditioner matrix; see Section 3.1 for more information on preconditioners. The last term is approximated with the SLQ method as follows:

$$\log \det(P^{-\frac{1}{2}}(\Sigma^{-1} + Z^T W Z)P^{-\frac{T}{2}}) \approx \frac{n}{t} \sum_{i=1}^t e_1^T \log(\tilde{T}_i) e_1, \quad (15)$$

where $z_1, \dots, z_t \in \mathbb{R}^m$ are i.i.d. random vectors with $\mathbb{E}[z_i] = 0$ and $\mathbb{E}[z_i z_i^T] = P$, $\tilde{Q}_i \tilde{T}_i \tilde{Q}_i^T \approx P^{-\frac{1}{2}}(\Sigma^{-1} + Z^T W Z)P^{-\frac{T}{2}}$ is a partial Lanczos decomposition obtained after l steps of the Lanczos algorithm with $P^{-\frac{1}{2}} z_i / \|P^{-\frac{1}{2}} z_i\|_2$ as initial vector, $\tilde{Q}_i \in \mathbb{R}^{m \times l}$ has orthonormal columns, $\tilde{T}_i \in \mathbb{R}^{l \times l}$ is tridiagonal, and $e_1 = (1, 0, \dots, 0)^T$. A derivation of this approximation can be found, e.g., in Kündig and Sigrist [2024, Appendix A.2]. In this article, we use Gaussian random vectors $z_i \sim \mathcal{N}(0, P)$. Wenger et al. [2022] highlight that a decomposition with a preconditioner as in (14) leads to a reduction in variance. Intuitively, the more accurate the preconditioner $P \approx (\Sigma^{-1} + Z^T W Z)$, the smaller $\log \det(P^{-\frac{1}{2}}(\Sigma^{-1} + Z^T W Z)P^{-\frac{T}{2}})$, and thus the smaller the variance of its stochastic approximation.

As in Gardner et al. [2018], we use a technique from Saad [2003] to calculate the partial Lanczos tridiagonal matrices $\tilde{T}_1, \dots, \tilde{T}_t$ from the coefficients of the preconditioned CG algorithm when solving

$(\Sigma^{-1} + Z^T W Z)^{-1} z_1, \dots, (W + \tilde{\Sigma}^{-1})^{-1} z_t$ t times; see Appendix A.6. In doing so, we avoid running the Lanczos algorithm, which brings multiple advantages: Numerical instabilities are not an issue, storing \tilde{Q}_i is not necessary, and the linear solves $(\Sigma^{-1} + Z^T W Z)^{-1} z_i$ can be reused in the stochastic trace estimation (STE) for calculating derivatives of the log-determinant, e.g., as follows:

$$\frac{\partial \log \det(\Sigma^{-1} + Z^T W Z)}{\partial \theta_k} \approx \frac{1}{t} \sum_{i=1}^t ((\Sigma^{-1} + Z^T W Z)^{-1} z_i)^T \frac{\partial(\Sigma^{-1} + Z^T W Z)}{\partial \theta_k} P^{-1} z_i.$$

Gradients can thus be calculated with minimal computational overhead once the likelihood is calculated. In Appendix A.4, we show in detail how to calculate derivatives of log-determinants with respect to θ , F , b^* , and ξ , using STE and a form of variance reduction with control variates based on the SSOR preconditioner introduced in the next section. Trace terms of the Fisher information in (7) can also be approximated with STE as follows:

$$\begin{aligned} \text{tr} \left(\Psi^{-1} \frac{\partial \Psi}{\partial \theta_k} \Psi^{-1} \frac{\partial \Psi}{\partial \theta_l} \right) &= \text{tr} \left((W - W Z (\Sigma^{-1} + Z^T W Z)^{-1} Z^T W) Z_k Z_k^T \right. \\ &\quad \left. (W - W Z (\Sigma^{-1} + Z^T W Z)^{-1} Z^T W) Z_l Z_l^T \right) \\ &\approx \frac{1}{t} \sum_{i=1}^t \left((Z_k Z_k^T W - Z_k Z_k^T W Z (\Sigma^{-1} + Z^T W Z)^{-1} Z^T W) z_i \right)^T \\ &\quad (W Z_l Z_l^T - W Z (\Sigma^{-1} + Z^T W Z)^{-1} Z^T W Z_l Z_l^T) z_i, \end{aligned} \quad (16)$$

where we use the Woodbury identity, $\frac{\partial \Psi}{\partial \theta_k} = Z_k Z_k^T$, and Gaussian random vectors $z_i \sim \mathcal{N}(0, I_n)$. Linear solves $(\Sigma^{-1} + Z^T W Z)^{-1} Z^T W z_i$ and $(\Sigma^{-1} + Z^T W Z)^{-1} Z^T W Z_l Z_l^T z_i$ in (16) can be computed with the CG method. In experiments, we have found that an alternative STE for the Fisher information given in Appendix A.5 leads to less accurate estimates than the STE in (16) (results not tabulated).

3.1 Preconditioners

Preconditioners reduce the variance of approximations of log-determinants and their derivatives and accelerate the convergence speed of the CG method. To practically use a matrix P as a preconditioner, we need to construct it, perform linear solves with it, calculate $\log \det(P)$, and sample from $\mathcal{N}(0, P)$ in a computationally efficient manner. In the following, we describe several preconditioners that we consider in this article.

3.1.1 SSOR preconditioner

The “symmetric successive over-relaxation” (SSOR) preconditioner is given by

$$P_{\text{SSOR}} = (L + D) D^{-1} (L + D)^T, \quad (17)$$

where D is a diagonal matrix with diagonal entries $(D)_{ii} = (\Sigma^{-1} + Z^T W Z)_{ii}$ and L is a strictly lower-triangular matrix with entries $(L)_{ij} = \mathbf{1}_{\{i > j\}} (\Sigma^{-1} + Z^T W Z)_{ij} = \mathbf{1}_{\{i > j\}} (Z^T W Z)_{ij}$ such that $\Sigma^{-1} + Z^T W Z = L + L^T + D$.

3.1.2 ZIC preconditioner

The zero fill-in incomplete Cholesky (ZIC) factorization reported in Appendix A.7 gives the ZIC preconditioner $P_{\text{ZIC}} = L L^T \approx \Sigma^{-1} + Z^T W Z$, where $L \in \mathbb{R}^{m \times m}$ is a sparse lower triangular matrix that has the same sparsity pattern as $\Sigma^{-1} + Z^T W Z$. Unfortunately, we sometimes observe breakdowns [Scott and Tüma, 2014], i.e., (clearly) negative numbers in the calculations of square roots.

3.1.3 Diagonal preconditioner

The diagonal preconditioner P_{Diag} is given by $P_{\text{Diag}} = \text{diag}((\Sigma^{-1} + Z^T W Z)_{ii})$. As mentioned in the introduction, this is currently the most popular preconditioner for the CG method for random effects models.

3.1.4 Other preconditioners

We additionally consider two low-rank preconditioners obtained by applying low-rank approximations to the matrix $Z^T W Z \approx L_k L_k^T$, $L_k \in \mathbb{R}^{m \times k}$ to obtain $P = \Sigma^{-1} + L_k L_k^T$. For these low-rank preconditioners, linear solves and log-determinants can be computed using the Woodbury matrix identity and the matrix determinant lemma, respectively, and the costs thus scale linearly with m . First, we apply the pivoted Cholesky decomposition [Harbrecht et al., 2012] to $Z^T W Z$ to obtain L_k and denote the resulting preconditioner as P_{Chol} . This is a state-of-the-art approach for Gaussian Process regression [Gardner et al., 2018]. Second, we apply a partial Lanczos algorithm to approximate $Z^T W Z \approx L_k L_k^T$ and denote the corresponding preconditioner as P_{Lanczos} .

3.2 Predictive variances

The computational bottleneck for prediction is the calculation of the posterior predictive variances $\text{diag}(\Omega_p)$ in (12). These are required for predictive distributions of the latent and response variables as well as for predictive means of non-Gaussian response variables. Calculating $\text{diag}(\Omega_p)$ requires solving n_p linear equation systems with the matrix $\Sigma^{-1} + Z^T W Z$. For high-dimensional crossed random effects and large n_p , solving these linear systems with the CG method can thus be computationally prohibitive. We develop and compare three solutions for this: two simulation-based methods relying on the CG method and an approach based on the preconditioned Lanczos algorithm.

3.2.1 Predictive variances using a stochastic estimator for the diagonal of a matrix

Bekas et al. [2007] propose to approximate the diagonal of a matrix $A \in \mathbb{R}^{n_p \times n_p}$ as $\text{diag}(A) \approx \frac{1}{s} \sum_{i=1}^s z_i \odot A z_i$, where \odot denotes the Hadamard product and $z_i \in \mathbb{R}^{n_p}$ are Rademacher random vectors with entries ± 1 . Algorithm 1 presents our method for calculating $\text{diag}(\Omega_p)$ by stochastically approximating $\text{diag}(Z_{po}(\Sigma^{-1} + Z^T W Z)^{-1} Z_{po}^T)$ in (12) based on the approach of Bekas et al. [2007]. Note that Gyger et al. [2024] have used a similar algorithm for predictive covariances in Gaussian process regression. Linear solves for the stochastic estimator are computed with the preconditioned CG method. We additionally apply variance reduction in Algorithm 1 by using a control variate based on $\text{diag}(Z_{po} P^{-1} Z_{po}^T)$:

$$\begin{aligned} \text{diag}(Z_{po}(\Sigma^{-1} + Z^T W Z)^{-1} Z_{po}^T) &\approx c \odot \text{diag}(Z_{po} P^{-1} Z_{po}^T) \\ &+ \frac{1}{t} \sum_{i=1}^t \underbrace{z_i \odot Z_{po}(\Sigma^{-1} + Z^T W Z)^{-1} Z_{po}^T z_i}_{=:h(z_i)} - c \odot \underbrace{z_i \odot Z_{po} P^{-1} Z_{po}^T z_i}_{=:r(z_i)}, \end{aligned}$$

where $c \in \mathbb{R}^{n_p}$ are the optimal weights for the variance reduction given by $c_j = \widehat{\text{Cov}}([h(z_i)]_j, [r(z_i)]_j) / \widehat{\text{Var}}([r(z_i)]_j)$, for $j = 1, 2, \dots, n_p$. This variance reduction is important as otherwise the variance of the stochastic approximation is much larger (results not tabulated). Algorithm 1 can be trivially parallelized and results in an unbiased and consistent approximation for $\text{diag}(\Omega_p)$; see Appendix A.3 for a proof of Proposition 3.1. Assuming that $P^{-\frac{1}{2}} Z_{po}^T$ is precomputed, $P = P^{\frac{1}{2}} P^{\frac{T}{2}}$, the computational complexity of the algorithm is $O(sn_p + slm + s\psi)$, where l denotes the number of CG iterations, s the number of simulation iterations, and ψ the number of non-zero entries in $P^{-\frac{1}{2}} Z_{po}^T$.

Algorithm 1 Approximate predictive variances using stochastic estimator for the diagonal of a matrix

Input: Matrices $Z_{po}, Z, \Sigma, Z_{pp}, \Sigma_p$, and W

Output: Approximate predictive variances $\text{diag}(\hat{\Omega}_p)$

- 1: **for** $i \leftarrow 1$ to s **do**
 - 2: Sample $z_i^{(1)} \stackrel{\text{i.i.d.}}{\sim}$ Rademacher, $z_i^{(1)} \in \mathbb{R}^{n_p}$
 - 3: $z_i^{(2)} \leftarrow Z_{po}(\Sigma^{-1} + Z^T W Z)^{-1} Z_{po}^T z_i^{(1)}$
 - 4: $z_i^{(3)} \leftarrow Z_{po} P^{-1} Z_{po}^T z_i^{(1)}$
 - 5: **end for**
 - 6: $c_j \leftarrow \widehat{\text{Cov}}((z_i^{(1)} \odot z_i^{(2)})_j, (z_i^{(1)} \odot z_i^{(3)})_j) / \widehat{\text{Var}}((z_i^{(1)} \odot z_i^{(3)})_j)$, $j = 1, 2, \dots, n_p$, $c = (c_1, \dots, c_{n_p})^T$
 - 7: $\text{diag}(\hat{\Omega}_p) \leftarrow \text{diag}(Z_{pp} \Sigma_p Z_{pp}^T) + c \odot \text{diag}(Z_{po} P^{-1} Z_{po}^T) + \frac{1}{s} \sum_{i=1}^s (z_i^{(1)} \odot z_i^{(2)} - c \odot z_i^{(1)} \odot z_i^{(3)})$
-

Proposition 3.1. *Algorithm 1 produces an unbiased and consistent estimator $\text{diag}(\hat{\Omega}_p)$ for the predictive variances $\text{diag}(\Omega_p)$ given in (12).*

We have also considered a similar algorithm using the alternative version in (11) for Ω_p instead of (12). Specifically, $\text{diag}(Z_{po}\Sigma Z^T \Psi^{-1} Z \Sigma Z_{po}^T)$ is approximated stochastically with the approach of Bekas et al. [2007] using the Woodbury identity, and all other terms are computed deterministically. However, experiments show that such an algorithm results in less accurate estimates compared to Algorithm 1 (results not tabulated).

3.2.2 Predictive covariances using simulation

Adopting an approach proposed in Kündig and Sigrist [2024], predictive covariances Ω_p can be approximated using expression (12) and sampling from a Gaussian distribution with covariance matrix $Z_{po}(\Sigma^{-1} + Z^T W Z)^{-1} Z_{po}^T$. Algorithm 2 presents this approach. The linear solves $(\Sigma^{-1} + Z^T W Z)^{-1} z_i^{(3)}$ can be done using the preconditioned CG method and the computational complexity of Algorithm 2 is thus $O(sn + slm + sn_p)$. This algorithm can also be trivially parallelized and results in an unbiased and consistent approximation for Ω_p ; see Appendix A.3 for a proof of Proposition 3.2. In contrast to Algorithm 1, this method can be used to calculate the entire covariance matrix and not just the variances on the diagonal. Furthermore, Algorithm 2 can be adapted to compute only the predictive variances $\text{diag}(\Omega_p)$ by summing $z_i^{(4)} \odot z_i^{(4)}$ in Line 5. We have also considered applying variance reduction to the estimator in Algorithm 2 by using a control variate based on $Z_{po} P^{-1} Z_{po}^T$. However, we found that the variance reduction was very small for predictive variances since $\widehat{\text{Cov}}((z_i^{(4)}(z_i^{(4)})^T)_{jk}, (z_i^{(5)}(z_i^{(5)})^T)_{jk})$, $z_i^{(5)} = Z_{po} P^{-\frac{T}{2}} z_i^{(1)}$ and $j, k = 1, 2, \dots, n_p$, is often close to zero.

Algorithm 2 Approximate predictive covariances using simulation

Input: Matrices $Z_{po}, Z, \Sigma, Z_{pp}, \Sigma_p$, and W

Output: Approximate predictive covariances $\hat{\Omega}_p$

- 1: **for** $i \leftarrow 1$ to s **do**
 - 2: Sample $z_i^{(1)} \stackrel{\text{i.i.d.}}{\sim} \mathcal{N}(0, I_m)$ and $z_i^{(2)} \stackrel{\text{i.i.d.}}{\sim} \mathcal{N}(0, I_n)$ and set $z_i^{(3)} \leftarrow \Sigma^{-\frac{1}{2}} z_i^{(1)} + Z^T W \frac{1}{2} z_i^{(2)}$
 - 3: $z_i^{(4)} \leftarrow Z_{po}(\Sigma^{-1} + Z^T W Z)^{-1} z_i^{(3)}$
 - 4: **end for**
 - 5: $\hat{\Omega}_p \leftarrow Z_{pp} \Sigma_p Z_{pp}^T + \frac{1}{s} \sum_{i=1}^s z_i^{(4)} (z_i^{(4)})^T$
-

Proposition 3.2. *Algorithm 2 produces an unbiased and consistent estimator $\hat{\Omega}_p$ for the predictive covariances Ω_p given in (12).*

Alternatively, we can use the expression in (11) and approximate $Z_{po}\Sigma Z^T \Psi^{-1} Z \Sigma Z_{po}^T$ using simulation. Algorithm 3 presents this approach. The linear solve $\Psi^{-1} z_i^{(3)}$ can be done using the Woodbury identity and the preconditioned CG method. The computational complexity of Algorithm 3 is thus $O(sn + slm + sn_p)$. This algorithm also results in an unbiased and consistent approximation for Ω_p ; see Appendix A.3 for a proof of Proposition 3.3.

Proposition 3.3. *Algorithm 3 produces an unbiased and consistent estimator $\hat{\Omega}_p$ for the predictive covariances Ω_p given in (11).*

Moreover, we can apply the Woodbury identity in (11) and obtain

$$Z_{po}\Sigma Z^T \Psi^{-1} Z \Sigma Z_{po}^T = Z_{po}\Sigma Z^T W Z \Sigma Z_{po}^T - Z_{po}\Sigma Z^T W Z (\Sigma^{-1} + Z^T W Z)^{-1} Z^T W Z \Sigma Z_{po}^T. \quad (18)$$

We have additionally considered an algorithm, where only the last term in (18) is approximated by simulation and all other terms in (11) are calculated deterministically. However, we observe in experiments that such an algorithm leads to less accurate estimates than when using Algorithm 2 and Algorithm 3 (results not tabulated).

Algorithm 3 Approximate predictive covariances using simulation

Input: Matrices $Z_{po}, Z, \Sigma, Z_{pp}, \Sigma_p$, and W

Output: Approximate predictive covariances $\hat{\Omega}_p$

- 1: **for** $i \leftarrow 1$ to s **do**
 - 2: Sample $z_i^{(1)} \stackrel{\text{i.i.d.}}{\sim} \mathcal{N}(0, I_m)$ and $z_i^{(2)} \stackrel{\text{i.i.d.}}{\sim} \mathcal{N}(0, I_n)$ and set $z_i^{(3)} \leftarrow Z\Sigma^{\frac{1}{2}}z_i^{(1)} + W^{-\frac{1}{2}}z_i^{(2)}$
 - 3: $z_i^{(4)} \leftarrow Z_{po}\Sigma Z^T\Psi^{-1}z_i^{(3)}$
 - 4: **end for**
 - 5: $\hat{\Omega}_p \leftarrow Z_{po}\Sigma Z_{po}^T + Z_{pp}\Sigma_p Z_{pp}^T - \frac{1}{s} \sum_{i=1}^s z_i^{(4)} \left(z_i^{(4)} \right)^T$
-

3.2.3 Predictive variances using preconditioned Lanczos algorithms

Pleiss et al. [2018] use the Lanczos algorithm to approximate predictive covariance matrices for Gaussian process regression. We adapt and extend this approach for GMMs. Specifically, we approximate $\text{diag}(Z_{po}\Sigma Z^T W Z(\Sigma^{-1} + Z^T W Z)^{-1} Z^T W Z \Sigma Z_{po}^T)$ in (18) by running the Lanczos algorithm with the matrix $\Sigma^{-1} + Z^T W Z$ using the normalized average of the column vectors of $Z^T W Z \Sigma Z_{po}^T$ as initial value and approximate $(\Sigma^{-1} + Z^T W Z)^{-1} Z^T W Z \Sigma Z_{po}^T \approx \tilde{Q}\tilde{T}^{-1}\tilde{Q}^T Z^T W Z \Sigma Z_{po}^T$, where $\tilde{Q}\tilde{T}\tilde{Q}^T \approx \Sigma^{-1} + Z^T W Z$ is obtained after k steps of the Lanczos algorithm, $\tilde{Q} \in \mathbb{R}^{n \times k}$ has orthonormal columns, and $\tilde{T} \in \mathbb{R}^{k \times k}$ is tridiagonal. $\text{diag}(Z_{po}\Sigma Z^T W Z \Sigma Z_{po}^T)$ and the other terms in (11) are deterministically computed, and predictive variances are thus approximated by

$$\begin{aligned} \text{diag}(\hat{\Omega}_p) &\approx \text{diag}(Z_{po}\Sigma Z_{po}^T) + \text{diag}(Z_{pp}\Sigma_p Z_{pp}^T) - \text{diag}(Z_{po}\Sigma Z^T W Z \Sigma Z_{po}^T) \\ &\quad + \text{diag}(Z_{po}\Sigma Z^T W Z \tilde{Q}\tilde{T}^{-1}\tilde{Q}^T Z^T W Z \Sigma Z_{po}^T). \end{aligned} \quad (19)$$

The computation of a rank k Lanczos approximation requires one matrix-vector multiplication with $\Sigma^{-1} + Z^T W Z$ in each iteration. Since the Lanczos algorithm suffers from numerical stability issues due to loss of orthogonality, we use a full reorthogonalization scheme [Wu and Simon, 2000]. Computing the Lanczos approximation then has complexity $O(k^2 m)$. Furthermore, we consider a similar way of preconditioning as in Kündig and Sigrist [2024] by applying the partial Lanczos algorithm to $P^{-\frac{1}{2}}(\Sigma^{-1} + Z^T W Z)P^{-\frac{T}{2}} \approx \tilde{Q}\tilde{T}\tilde{Q}$ and correcting for this by using $P^{-\frac{T}{2}}\tilde{Q}\tilde{T}^{-1}\tilde{Q}P^{-\frac{1}{2}}Z^T W Z \Sigma Z_{po}^T \approx (\Sigma^{-1} + Z^T W Z)^{-1} Z^T W Z \Sigma Z_{po}^T$ as approximation. Note that the Lanczos algorithm requires a symmetric matrix and in contrast to the preconditioned CG method, we need to explicitly calculate a factor $P^{-\frac{1}{2}}$, where $P = P^{\frac{1}{2}}P^{\frac{T}{2}}$. This is possible for the diagonal, SSOR, and ZIC preconditioners. However, in our experiments, this form of preconditioning does not lead to more accurate predictive variance estimates (results not tabulated).

3.3 Software implementation

The methods presented in this article are implemented in the GPBoost library written in C++ with Python and R interfaces, see <https://github.com/fabsig/GPBoost>.^{*} For linear algebra calculations, we use the Eigen library version 3.4.99 and its sparse matrix algebra operations whenever possible. Multi-processor parallelization is done using OpenMP.

4 Convergence analysis

In the following, we theoretically analyze the properties of the Krylov subspace methods presented in this article. We denote by $\lambda_{\min} = \lambda_m \leq \dots \leq \lambda_1 = \lambda_{\max}$ the eigenvalues of a symmetric matrix $A \in \mathbb{R}^{m \times m}$. The eigenvalues of the preconditioned matrix $P^{-1/2}(\Sigma^{-1} + Z^T W Z)P^{-T/2}$ determine the convergence speed and accuracy of the CG and SLQ methods. However, there are important difference among the two methods. It is known that the CG method converges fast if the majority of the eigenvalues are clustered together and an effective condition number $\kappa_{m-l,k} = \frac{\lambda_k}{\lambda_{m-l}}$ [Van der Sluis and van der Vorst, 1986] is small for small $k, l \geq 1$, despite the presence of a few outlying small

^{*}Krylov subspace methods can be enabled via the parameter `matrix_inversion_method = "iterative"` and the preconditioner is chosen via the parameter `cg_preconditioner.type`.

and large eigenvalues; see, e.g., [Van der Vorst \[2003\]](#) and [Nishimura and Suchard \[2022\]](#). In particular, a large condition number $\kappa = \frac{\lambda_{\max}}{\lambda_{\min}}$ is not necessarily a problem for the convergence speed of the CG method. [Pandolfi et al. \[2024\]](#) have recently shown that, for the diagonal preconditioner and a Gaussian likelihood, the majority of the eigenvalues of $P^{-1/2}(\Sigma^{-1} + Z^T W Z)P^{-T/2}$ are clustered together except for a few small eigenvalues. This likely explains the relatively popular application of the diagonal preconditioner for the CG method in the prior literature [[Tsuruta et al., 2001](#), [Taskinen et al., 2017](#), [Garrrick et al., 2019](#), [Pandolfi et al., 2024](#)]. In line with this, our experiments in Section 5 show that the CG method, whether used with the diagonal, SSOR, or ZIC preconditioner, or even without preconditioning, yields similar runtimes.

The situation is different for the SLQ method. Here, the smallest and largest eigenvalues, λ_{\min} and λ_{\max} , are important for its convergence properties and accuracy as outlined in the following. In brief, the Lanczos algorithm factorizes a symmetric matrix as $A = QTQ^T$, where $Q \in \mathbb{R}^{n \times n}$ is orthonormal, and $T \in \mathbb{R}^{n \times n}$ is a tridiagonal matrix. This decomposition is computed iteratively, and k iterations result in an approximation $A \approx \tilde{Q}\tilde{T}\tilde{Q}^T$, where $\tilde{Q} \in \mathbb{R}^{n \times k}$ contains the first k columns of Q , and $\tilde{T} \in \mathbb{R}^{k \times k}$ the corresponding coefficients of T . Using $\log \det(A) = \text{tr} \log(A)$ and $\log(A) \approx \tilde{Q} \log(\tilde{T}) \tilde{Q}^T$, SLQ then applies stochastic trace estimation to approximate $\log \det(A)$; see (15), [Ubaru et al. \[2017\]](#), and [Kündig and Sigrist \[2024, Appendix A.2\]](#) for more details. The logarithm function used in $\log(A) \approx \tilde{Q} \log(\tilde{T}) \tilde{Q}^T$ is mostly determined by the extremal eigenvalues of $A = P^{-1/2}(\Sigma^{-1} + Z^T W Z)P^{-T/2}$. Furthermore, it is known that the Lanczos algorithm approximates the smallest eigenvalue λ_m faster when the difference $\lambda_1 - \lambda_m$ is smaller and when $\frac{\lambda_{m-1} - \lambda_m}{\lambda_1 - \lambda_{m-1}}$ is larger [[Golub and Van Loan, 2013](#)]. Similarly, the largest eigenvalue λ_1 is approximated the faster, the smaller $\lambda_1 - \lambda_m$ and the larger $\frac{\lambda_1 - \lambda_2}{\lambda_2 - \lambda_m}$. Similar results can also be obtained for other eigenvalues. This means that the difference between the largest and smallest eigenvalues matters much more for the SLQ method compared to the CG method. In line with this, we find in our experiments in Section 5 that preconditioners for which the difference between the largest and smallest eigenvalues is small, such as the SSOR preconditioner, result in much more accurate log-determinant approximations compared to the diagonal preconditioner for which this difference is larger.

In addition to the above-mentioned intuitive and empirical arguments, there is convergence theory showing that the error of an SLQ-approximated log-determinant depends on the condition number $\kappa = \lambda_1/\lambda_m$ of $P^{-1/2}(\Sigma^{-1} + Z^T W Z)P^{-T/2}$. Below, we restate Theorem 3.2 of [Kündig and Sigrist \[2024\]](#) for our setting, which provides a stochastic error bound. We are not aware of any convergence results that relate an effective condition number $\kappa_{m-l,k} = \lambda_k/\lambda_{m-l}$ to the approximation error of an SLQ-approximated log-determinant.

Theorem 4.1. *Let $\kappa = \frac{\lambda_1}{\lambda_m}$ denote the condition number of $P^{-1/2}(\Sigma^{-1} + Z^T W Z)P^{-T/2}$, $C_{mt} = \frac{Q_{\chi_{mt}^2, (1-\eta/2)}}{mt}$, where $Q_{\chi_{mt}^2}(\cdot)$ is the quantile function of a χ^2 -distribution with mt degrees of freedom, and $\hat{\Gamma} = \frac{1}{t} \sum_{i=1}^t \|P^{-\frac{1}{2}} z_i\|_2^2 e_1^T \log(\tilde{T}_i) e_1$ an SLQ approximation. If the SLQ method is run with $l \geq \frac{\sqrt{3\kappa}}{4} \log\left(\frac{C_{mt} 20 \log(2(\kappa+1)) \sqrt{2\kappa+1}}{\epsilon}\right)$ preconditioned CG steps and $t \geq \frac{32}{\epsilon^2} \log(\kappa+1)^2 \log\left(\frac{4}{\eta}\right)$ number of random vectors, the following holds for any preconditioner P :*

$$P(|\hat{\Gamma} - \log \det(P^{-1/2}(\Sigma^{-1} + Z^T W Z)P^{-T/2})| \leq \epsilon m) \geq 1 - \eta, \quad (20)$$

where $\epsilon, \eta \in (0, 1)$.

In the following, we analyze the extremal eigenvalues of the preconditioned matrices $P^{-1/2}(\Sigma^{-1} + Z^T W Z)P^{-T/2}$ for different preconditioners P . We denote by $\lambda_{\min}^P = \lambda_m^P \leq \dots \leq \lambda_1^P = \lambda_{\max}^P$ the eigenvalues of $P^{-1/2}(\Sigma^{-1} + Z^T W Z)P^{-T/2}$ for a preconditioner P . In addition, the eigenvalues of the non-preconditioned matrix $\Sigma^{-1} + Z^T W Z$ are denoted by $\lambda_{\min}^{\text{none}} = \lambda_m^{\text{none}} \leq \dots \leq \lambda_1^{\text{none}} = \lambda_{\max}^{\text{none}}$.

4.1 SSOR preconditioner

Theorem 4.2 and Corollary 4.1 derive the extremal eigenvalues, as well as lower and upper bounds, of the SSOR-preconditioned matrix $P_{\text{SSOR}}^{-1/2}(\Sigma^{-1} + Z^T W Z)P_{\text{SSOR}}^{-T/2}$, for general non-Gaussian and Gaussian likelihoods, respectively. In particular, Theorem 4.2 and Corollary 4.1 imply that the largest and smallest eigenvalues, $\lambda_{\max}^{\text{SSOR}}$ and $\lambda_{\min}^{\text{SSOR}}$, of $P_{\text{SSOR}}^{-1/2}(\Sigma^{-1} + Z^T W Z)P_{\text{SSOR}}^{-T/2}$ do not depend directly on neither the sample size n nor the dimension of the random effects m but rather only on the number

of repeated observations per random effect, denoted by $d = \frac{n}{m_1} = \frac{n}{m_2}$ when having a balanced design. Furthermore, the results show that the ratio $\lambda_{\max}^{\text{SSOR}}/\lambda_{\min}^{\text{SSOR}}$ and the difference between the largest and smallest eigenvalues of $P_{\text{SSOR}}^{-1/2}(\Sigma^{-1} + Z^T W Z)P_{\text{SSOR}}^{-T/2}$ are increasing in the number of repeated observations per random effect; see, e.g., (26).

Theorem 4.2. Denote $D_1 = \text{diag}((\Sigma^{-1} + Z^T W Z)_{ii}) \in \mathbb{R}^{m_1 \times m_1}$ and $D_2 = \text{diag}((\Sigma^{-1} + Z^T W Z)_{ii}) \in \mathbb{R}^{(m-m_1) \times (m-m_1)}$. If $K = 2$, the following hold true for the SSOR preconditioner defined in Section 3.1.1:

$$P_{\text{SSOR}}^{-1/2}(\Sigma^{-1} + Z^T W Z)P_{\text{SSOR}}^{-T/2} = I_m - \begin{pmatrix} 0 & 0 \\ 0 & D_2^{-1/2} Z_2^T W Z_1 D_1^{-1} Z_1^T W Z_2 D_2^{-1/2} \end{pmatrix}, \quad (21)$$

$$\lambda_{m_1}^{\text{SSOR}} = \dots = \lambda_1^{\text{SSOR}} = \lambda_{\max}^{\text{SSOR}} = 1, \quad (22)$$

$$1 - \frac{1}{(\min(\Sigma_{ii}^{-1}(Z^T W Z)_{ii}^{-1}) + 1)^2} \leq \lambda_{\min}^{\text{SSOR}} \leq 1 - \frac{1}{(\max(\Sigma_{ii}^{-1}(Z^T W Z)_{ii}^{-1}) + 1)^2}, \quad (23)$$

$$1 - \max((D_1^{-1})_{ii}) \max((D_2^{-1})_{ii}) \max((Z^T W Z)_{ii})^2 \leq \lambda_{\min}^{\text{SSOR}} \leq 1 - \min((D_1^{-1})_{ii}) \min((D_2^{-1})_{ii}) \min((Z^T W Z)_{ii})^2. \quad (24)$$

A proof of Theorem 4.2 can be found in Appendix A.1. Theorem 4.2 implies the following corollary for Gaussian likelihoods.

Corollary 4.1. If $K = 2$ and the likelihood is Gaussian, it holds that

$$\lambda_{m_1}^{\text{SSOR}} = \dots = \lambda_1^{\text{SSOR}} = \lambda_{\max}^{\text{SSOR}} = 1, \\ 1 - \left(\frac{\max(\sigma_1^2, \sigma_2^2) d^{\max}}{\sigma^2 + \max(\sigma_1^2, \sigma_2^2) d^{\max}} \right)^2 \leq \lambda_{\min}^{\text{SSOR}} \leq 1 - \left(\frac{\min(\sigma_1^2, \sigma_2^2) d^{\min}}{\sigma^2 + \min(\sigma_1^2, \sigma_2^2) d^{\min}} \right)^2, \quad (25)$$

where $d^{\max} = \max(Z^T Z)$ and $d^{\min} = \min(Z^T Z)$ are the largest and smallest number of repeated measurements for the two grouped random effects, respectively.

If, in addition, the design of the random effects is balanced such that every random effect realization occurs d times, i.e., $d = \frac{n}{m_k} = \sum_{i=1}^n (Z_k)_{ij}$ for all $1 \leq j \leq m_k$ and $k = 1, 2$, the following holds true:

$$\lambda_{\min}^{\text{SSOR}} = 1 - \left(\frac{1}{\frac{\sigma^2}{\sigma_1^2 d} + 1} \right) \left(\frac{1}{\frac{\sigma^2}{\sigma_2^2 d} + 1} \right) \quad (26)$$

Proof of Corollary 4.1. The statement in (25) follows from (23). Similarly, (26) follows from (24) by plugging in $D_k = \text{diag}(1/\sigma_k^2 + d_k/\sigma^2)$, $k = 1, 2$. \square

When making additional assumptions on the random effects design, we can derive a lower bound for the second smallest eigenvalue $\lambda_{m-1}^{\text{SSOR}}$ in Theorem 4.3 below. Theorem 4.3 shows that the effective condition number $\kappa_{m-1,1}^{\text{SSOR}} = \lambda_1^{\text{SSOR}}/\lambda_{m-1}^{\text{SSOR}}$ decreases fast to one as the number of occurrences per random effect d_k increases. Consequently, the preconditioned CG method is expected to converge faster for larger d_k ; see the discussion at the beginning of Section 4. Note that the assumptions of Theorem 4.3, which are the same as in Pandolfi et al. [2024, Section 5.4.1], imply that the random effects design is balanced in the sense that every random effect realization occurs d_k times for $k = 1, 2$, $d_k = \frac{n}{m_k} = \sum_{i=1}^n (Z_k)_{ij}$, $\forall 1 \leq j \leq m_k$, and that all pairs of elements of $b_1 \in \mathbb{R}^{m_1}$ and $b_2 \in \mathbb{R}^{m_2}$, $b = (b_1^T, b_2^T)^T$, co-occur at most once in all observations, i.e., $Z_2^T Z_1 \in \{0, 1\}^{m_2 \times m_1}$.

Theorem 4.3. If $K = 2$, the likelihood is Gaussian, and $\begin{pmatrix} 0 & Z_1^T Z_2 \\ Z_2^T Z_1 & 0 \end{pmatrix} \in \{0, 1\}^{m \times m}$ is an adjacency matrix of a bipartite, biregular random graph with uniform distribution over all bipartite, biregular random graphs, the following hold:

$$\lambda_{m-1}^{\text{SSOR}} \geq 1 - \frac{(\sqrt{d_1 - 1} + \sqrt{d_2 - 1})^2}{(\sigma^2/\sigma_1^2 + d_1)(\sigma^2/\sigma_2^2 + d_2)} - \epsilon_m \quad (27)$$

and

$$\kappa_{m-1,1}^{\text{SSOR}} = \frac{\lambda_1^{\text{SSOR}}}{\lambda_{m-1}^{\text{SSOR}}} \leq \frac{1}{1 - \left(\frac{1}{d_1} + \frac{1}{d_2} + \frac{2}{\sqrt{d_1 d_2}} \right) - \epsilon_m} \quad (28)$$

asymptotically almost surely with $\epsilon_m \rightarrow 0$ as $m \rightarrow \infty$, where $d_k = \frac{n}{m_k}$ for $k = 1, 2$.

A proof of Theorem 4.3 can be found in Appendix A.1. Pandolfi et al. [2024, Theorem 4] derive a similar result for the diagonal preconditioner. However, the upper bound for the effective condition number $\kappa_{m-1,1}^{\text{SSOR}}$ of the SSOR-preconditioned matrix given by $1/(1 - (\frac{1}{d_1} + \frac{1}{d_2} + \frac{2}{\sqrt{d_1 d_2}}) - \epsilon_m)$ decreases faster than the corresponding upper bound $(1 + \frac{1}{\sqrt{d_1}} + \frac{1}{\sqrt{d_2}} + \epsilon_m)/(1 - (\frac{1}{\sqrt{d_1}} + \frac{1}{\sqrt{d_2}}) - \epsilon_m)$ for the diagonal preconditioner derived in Pandolfi et al. [2024, Theorem 4]; see Section 4.3 for more details. Note that the random effects model used in Pandolfi et al. [2024] contains a random intercept term, which we do not include, and they derive their result for $\kappa_{m-2,3}^{\text{Diag}}$ instead of $\kappa_{m-1,1}^{\text{Diag}}$. However, in Theorem A.1 in Appendix A.2, we show that the same result holds true for $\kappa_{m-1,1}^{\text{Diag}}$ for the model without a random intercept used in this article.

4.2 Diagonal preconditioner and no preconditioner

We have the following results for the diagonal preconditioner and the non-preconditioned matrix $\Sigma^{-1} + Z^T W Z$. We comment on these results and compare them in Section 4.3.

Theorem 4.4. *For the diagonal preconditioner $P_{\text{Diag}} = D$, it holds that*

$$1 + \frac{K-1}{\max(\Sigma_{ii}^{-1}(Z^T W Z)_{ii}^{-1}) + 1} \leq \lambda_{\max}^{\text{Diag}} \leq 1 + \frac{K-1}{\min(\Sigma_{ii}^{-1}(Z^T W Z)_{ii}^{-1}) + 1}, \quad (29)$$

$$\frac{1}{\max(\Sigma_{ii} D_{ii})} \leq \lambda_{m+1-k}^{\text{Diag}} \leq \frac{1}{\min(\Sigma_{ii} D_{ii})}, \quad k = 1, \dots, K-1. \quad (30)$$

If the likelihood is Gaussian, we can additionally obtain the following result.

Theorem 4.5. *If the likelihood is Gaussian, it holds that*

$$1 + \frac{K-1}{\frac{\max(\Sigma^{-1})\sigma^2}{d^{\min}} + 1} \leq \lambda_{\max}^{\text{Diag}} \leq 1 + \frac{K-1}{\frac{\min(\Sigma^{-1})\sigma^2}{d^{\max}} + 1}, \quad (31)$$

$$\frac{1}{\frac{\max(\Sigma)}{\sigma^2} d^{\max} + 1} \leq \lambda_{m+1-k}^{\text{Diag}} \leq \frac{1}{\frac{\min(\Sigma)}{\sigma^2} d^{\min} + 1}, \quad k = 1, \dots, K-1, \quad (32)$$

where $d^{\max} = \max(Z^T Z)$ and $d^{\min} = \min(Z^T Z)$.

If, in addition, $K = 2$ and the design of the random effects is balanced such that every random effect realization occurs d_k times, i.e., $d_k = \frac{n}{m_k} = \sum_{i=1}^n (Z_k)_{ij}$ for all $1 \leq j \leq m_k$ and $k = 1, 2$, it holds that

$$\lambda_{\max}^{\text{Diag}} = 1 + \frac{1}{\sqrt{\left(\frac{\sigma^2}{\sigma_1^2 d_1} + 1\right) \left(\frac{\sigma^2}{\sigma_2^2 d_2} + 1\right)}} \quad (33)$$

$$\lambda_{\min}^{\text{Diag}} = 1 - \frac{1}{\sqrt{\left(\frac{\sigma^2}{\sigma_1^2 d_1} + 1\right) \left(\frac{\sigma^2}{\sigma_2^2 d_2} + 1\right)}} \quad (34)$$

Theorem 4.6. *The following hold true for the non-preconditioned matrix $\Sigma^{-1} + Z^T W Z$:*

$$\frac{1}{\max(\Sigma_{ii})} + K \min((Z^T W Z)_{ii}) \leq \lambda_{\max}^{\text{none}} \leq \frac{1}{\min(\Sigma_{ii})} + K \max((Z^T W Z)_{ii}), \quad (35)$$

$$\frac{1}{\max(\Sigma_{ii})} \leq \lambda_{m+1-k}^{\text{none}} \leq \frac{1}{\min(\Sigma_{ii})}, \quad k = 1, \dots, K-1. \quad (36)$$

Proofs of Theorems 4.4, 4.5, and 4.6 can be found in Appendix A.1.

4.3 Comparison of preconditioners

The above results show that the largest and smallest eigenvalues of $P^{-1/2}(\Sigma^{-1} + Z^T W Z)P^{-T/2}$ for the SSOR, the diagonal, and no preconditioner depend only on the number of repeated observations per random effect, denoted by $d_k = \frac{n}{m_k}$ when having a balanced design, and not directly on neither the sample size n nor the dimension m of $\Sigma^{-1} + Z^T W Z$. In the following, we analyze and compare the extremal eigenvalues and condition numbers of the preconditioned matrices in more detail.

Theorem 4.7 below demonstrates that, for $K = 2$, a Gaussian likelihood, and a balanced design with $d = m_1/m_2$ repeated observations per random effect, the condition numbers $\kappa = \lambda_1/\lambda_m$ for the SSOR and diagonal preconditioners and also when not applying any preconditioner grow asymptotically linearly in d . In detail, Theorem 4.7 shows that the condition number and the difference of the largest and smallest eigenvalue of the preconditioned matrix $P^{-1/2}(\Sigma^{-1} + Z^T W Z)P^{-T/2}$, which matter for SLQ, are smaller for the SSOR preconditioner compared to the diagonal preconditioner. Furthermore, the theorem shows that the condition number $\lambda_{\max}^{\text{SSOR}}/\lambda_{\min}^{\text{SSOR}}$ of the SSOR-preconditioned matrix has a linear asymptote in d with a slope that is four times smaller than the corresponding slope of the diagonal preconditioner. In other words, the condition number of the diagonal-preconditioned matrix grows four times faster in d than the one of the SSOR-preconditioned matrix. Based on this, we expect the SSOR preconditioner to result in more accurate SLQ-approximated log-determinants compared to the diagonal preconditioner. This is confirmed empirically in Section 5.

Furthermore, we can obtain an explicit expression for the condition number of the non-preconditioned matrix $\Sigma^{-1} + Z^T W Z$ if the two random effects have equal variances, $\sigma_1^2 = \sigma_2^2$ as the corresponding inequalities in Theorem 4.7 then become equalities. In this case, the condition number of the non-preconditioned and the diagonal-preconditioned matrix are equal and given by $\frac{2\sigma_1^2}{\sigma_1^2}d + 1$, whereas the condition number of the SSOR-preconditioned matrix asymptotically grows with a rate of $\frac{\sigma_1^2}{2\sigma_1^2}$ in d . For the diagonal preconditioner, this can be seen by noting that $\lambda_{\max}^{\text{Diag}}/\lambda_{\min}^{\text{Diag}} = ((\frac{\sigma_1^2}{\sigma_1^2}d + 1) + 1)/((\frac{\sigma_1^2}{\sigma_1^2}d + 1) - 1) = \frac{2\sigma_1^2}{\sigma_1^2}d + 1$ due to (49) in the proof of Theorem 4.7 in Appendix A.1. We conjecture that similar results also hold for the non-preconditioned matrix and the diagonal preconditioner for the general case $\sigma_1^2 \neq \sigma_2^2$.

Theorem 4.7. *If $K = 2$, the likelihood is Gaussian, and the random effects have a balanced design with $d = d_1 = \frac{n}{m_1} = d_2 = \frac{n}{m_2}$ repeated observations per random effect, the following hold true:*

$$\lambda_{\max}^{\text{SSOR}} < \lambda_{\max}^{\text{Diag}}, \quad \lambda_{\min}^{\text{SSOR}} > \lambda_{\min}^{\text{Diag}}, \quad (37)$$

$$\lim_{d \rightarrow \infty} \left(\frac{\lambda_{\max}^{\text{SSOR}}}{\lambda_{\min}^{\text{SSOR}}} - \left(\frac{\sigma_1^2 \sigma_2^2}{\sigma^2(\sigma_1^2 + \sigma_2^2)} d + 1 \right) \right) = 0, \quad (38)$$

$$\lim_{d \rightarrow \infty} \left(\frac{\lambda_{\max}^{\text{Diag}}}{\lambda_{\min}^{\text{Diag}}} - \left(\frac{4\sigma_1^2 \sigma_2^2}{\sigma^2(\sigma_1^2 + \sigma_2^2)} d + 1 \right) \right) = 0, \quad (39)$$

$$\frac{2 \min(\sigma_1^2, \sigma_2^2)}{\sigma^2} d + \frac{\min(\sigma_1^2, \sigma_2^2)}{\max(\sigma_1^2, \sigma_2^2)} \leq \frac{\lambda_{\max}^{\text{none}}}{\lambda_{\min}^{\text{none}}} \leq \frac{2 \max(\sigma_1^2, \sigma_2^2)}{\sigma^2} d + \frac{\max(\sigma_1^2, \sigma_2^2)}{\min(\sigma_1^2, \sigma_2^2)}, \quad (40)$$

We can additionally obtain upper bounds for the effective condition numbers $\kappa_{m-1,1}^{\text{SSOR}}$ and $\kappa_{m-1,2}^{\text{Diag}}$ for the SSOR and diagonal preconditioner, respectively, and a Gaussian likelihood when assuming that $\begin{pmatrix} 0 & Z_1^T Z_2 \\ Z_2^T Z_1 & 0 \end{pmatrix} \in \{0, 1\}^{m \times m}$ is an adjacency matrix of a bipartite, biregular random graph.

Theorem 4.8 below shows that the effective condition number $\kappa_{m-1,1}^{\text{SSOR}}$ of the SSOR-preconditioned matrix essentially decreases with a rate of $\frac{4}{d}$, up to higher-order terms. In contrast, the effective condition number $\kappa_{m-1,2}^{\text{Diag}}$ of the diagonal preconditioner decreases with a slower rate of $\frac{4}{\sqrt{d}}$, again up to higher-order terms. Note that the assumption $m_1 = m_2$ in Theorem 4.8 allows for simpler results but can be easily relaxed. Based on these results, we expect the SSOR preconditioner to lead to faster convergence of the CG method compared to the diagonal preconditioner. A proof of Theorem 4.8 can be found in Appendix A.2.

Theorem 4.8. *If $K = 2$, the likelihood is Gaussian, $m_1 = m_2$, and $\begin{pmatrix} 0 & Z_1^T Z_2 \\ Z_2^T Z_1 & 0 \end{pmatrix} \in \{0, 1\}^{m \times m}$ is an adjacency matrix of a bipartite, biregular random graph with uniform distribution over all bipartite, biregular random graphs, the following hold:*

$$\kappa_{m-1,1}^{\text{SSOR}} = \frac{\lambda_1^{\text{SSOR}}}{\lambda_{m-1}^{\text{SSOR}}} \leq \frac{1}{1 - \frac{4}{d} - \epsilon_m} = 1 + \frac{4}{d} + \epsilon_m + O\left(\frac{1}{d^2}, \epsilon_m^2, \frac{\epsilon_m}{d}\right), \quad (41)$$

$$\kappa_{m-1,2}^{\text{Diag}} = \frac{\lambda_2^{\text{Diag}}}{\lambda_{m-1}^{\text{Diag}}} \leq \frac{1 + \frac{2}{\sqrt{d}} + \epsilon'_m}{1 - \frac{2}{\sqrt{d}} - \epsilon'_m} = 1 + \frac{4}{\sqrt{d}} + 2\epsilon'_m + O\left(\frac{1}{d}, \epsilon_m^2, \frac{\epsilon'_m}{\sqrt{d}}\right) \quad (42)$$

asymptotically almost surely with $\epsilon_m \rightarrow 0$ and $\epsilon'_m \rightarrow 0$ as $m \rightarrow \infty$.

5 Experiments using simulated data

In the following, we conduct several experiments using simulated data. We compare the different preconditioners and methods for calculating predictive variances. Furthermore, we analyze our proposed methods concerning the accuracy and runtime for parameter estimation and prediction. Krylov subspace methods are compared to calculations based on the Cholesky decomposition using the `GPBoost` library. Note, however, that the Cholesky decomposition is also not exact since round-off errors can accumulate when using finite precision arithmetic. Additionally, we do a comparison with the `lme4` and `glmmTMB` software libraries, which both rely on the Cholesky decomposition. Code to reproduce the simulated and the real-world data experiments of this article is available at <https://github.com/pkuendig/KrylovGMMs>.

5.1 Experimental setting

We simulate data from a model with two randomly crossed random effects. Unless stated otherwise, we use a balanced random effects design, in which both random effects have the same dimension $m_1 = m_2$, and the random effect variances are $\sigma_1^2 = \sigma_2^2 = 0.25$. But we also conduct experiments for an unbalanced design and other choices of random effects variances. We include a linear regression fixed effects term with five covariates plus an intercept for simulation, estimation, and prediction. The covariates are sampled from a normal distribution with mean zero and variance chosen such that the signal-to-noise ratio between the fixed and random effects is one, and the true regression coefficients are all one except for the intercept, which is zero. The response variable y follows either a Gaussian likelihood with variance $\sigma^2 = 0.25$ or a Bernoulli likelihood with a logit link function. More details, e.g., on the sample size n and the dimension m of the random effects, are provided in the subsections below.

For analyzing prediction accuracy, the data is randomly split into training and test data sets. We measure both the accuracy of point and probabilistic predictions for the test data random effects $\tilde{b}_p = Z_{po}b + Z_{pp}b_p$; see (8). Point predictions in the form of predictive means are evaluated using the root mean squared error (RMSE), and for probabilistic predictions, we use the log score (LS) $-\frac{1}{n_p} \sum_{i=1}^{n_p} \log(\mathcal{N}((\tilde{b}_p)_i; \omega_{p,i}, (\Omega_p)_{ii}))$, where $\omega_{p,i}$ and $(\Omega_p)_{ii}$ are the predictive latent means and variances for the random effect $(\tilde{b}_p)_i$ of test observation i , and $\mathcal{N}((\tilde{b}_p)_i; \omega_{p,i}, (\Omega_p)_{ii})$ denotes a Gaussian density evaluated at $(\tilde{b}_p)_i$. We also measure the runtime in seconds.

All calculations are done on a laptop with an Intel i7-12800H processor and 32 GB of random-access memory. We use the `GPBoost` library version 1.5.8 for Krylov subspace and Cholesky decomposition-based methods denoted as ‘Krylov (GPBoost)’ and ‘Cholesky (GPBoost)’, respectively. Cholesky-based calculations are additionally done with the R packages `lme4` version 1.1-35.5 and `glmmTMB` version 1.1.10. For Gaussian likelihoods, parameter estimation is done by minimizing the negative log-marginal likelihood. For non-Gaussian likelihoods, all implementations use the Laplace approximation. For parameter estimation, we set the initial values for all models to the default values used by `GPBoost`. Besides the above-mentioned points, the default options of the packages are used, including package-specific internal optimizers.

For the Krylov subspace methods, if not stated otherwise, we use the SSOR preconditioner, set the number of random vectors for STE and SLQ to $t = 50$, and use a rank of $k = 50$ for the two low-rank preconditioners. For the CG algorithm, we use a convergence tolerance of 10^{-2} for calculating marginal likelihoods and gradients, and a tolerance of 10^{-3} for predictive variances. Unless stated otherwise, we use the Algorithm 1 and $s = 1000$ samples for calculating predictive variances. Further, we adopt a sample average approximation approach [Kim et al., 2015] when maximizing the marginal likelihood.

5.2 Preconditioner comparison

First, we compare the proposed preconditioners with regard to the accuracy and runtime for approximating log-marginal likelihoods. We set the total number of group levels to $m = 100'000$, use a sample size of $n = 1'000'000$, and consider varying numbers of random vectors t for the SLQ method. Note that these dimensions are approximately the largest ones such that Cholesky-based computations can

be run in a “reasonable” amount of time which is roughly four hours for one likelihood evaluation. For each preconditioner and number of random vectors, the calculation of the likelihood is done at the true covariance parameters and repeated 100 times with different random vectors. Figure 2 reports the results when the response variable follows a Gaussian likelihood. The runtime reported is the average wall-clock time. We first observe that the SSOR and ZIC preconditioners yield very accurate log-likelihood approximations with much smaller variances compared to the diagonal, Lanczos, and pivoted Cholesky preconditioners. This observation is consistent with the theoretical results presented in Section 4. Furthermore, we find that computations based on Krylov subspace methods are much faster than Cholesky-based computations. For instance, when using $t = 50$ random vectors, we obtain a speed-up of approximately four orders of magnitude. Moreover, the runtimes of the CG method are similar for all preconditioners and even without preconditioning. In line with our convergence theory, the diagonal preconditioner has slightly longer runtimes compared to the SSOR preconditioner, but the differences are small. We conjecture that the finding that the preconditioned and non-preconditioned CG methods have similar runtimes can, partially, be explained by computational overheads of the preconditioners and other computations. The longest runtimes are observed for the Lanczos preconditioner. In summary, while preconditioning does not reduce the runtime, it can substantially reduce the variance of log-marginal likelihoods. In particular, variance reduction is very effective with the SSOR and ZIC preconditioner but has no clear effect with the diagonal, Lanczos, and pivoted Cholesky preconditioners.

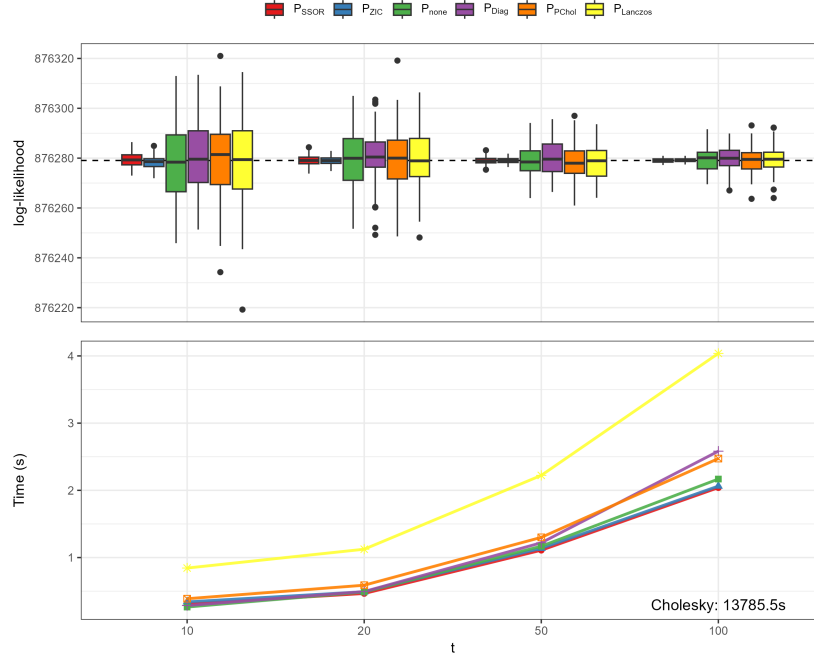


Figure 2: Negative log-marginal likelihood and wall-clock time in seconds for different preconditioners and numbers of random vectors t when the response variable follows a Gaussian likelihood. The dashed line represents the result for the Cholesky decomposition.

In Figure 9 in Appendix A.8, we report analogous results when the response variable follows a Bernoulli likelihood with a logit link function and all other settings are identical for the SSOR, ZIC, and diagonal preconditioners. Similar observations can be made in this non-Gaussian setting, with the SSOR and ZIC preconditioners having substantially smaller variances than the diagonal preconditioner. Furthermore, in Figure 10 in Appendix A.8, we report the results when using an unbalanced random-effects design with $m_2 = \frac{m_1}{2}$, and in Figure 11 in Appendix A.8 we present the results when having a different signal-to-noise ratio with $\sigma_1^2 = \sigma_2^2 = 1$ for a Gaussian likelihood. The results for these two settings are again very similar to the previous ones. Cholesky-based computations are faster for the unbalanced design, since $Z^T W Z$ is more sparse, but still three orders of magnitude slower than Krylov subspace methods. Note that the experiments in this section and the following Section 5.3 are conducted on only one simulated data set since we do not want to mix sampling variability and

variability of the simulation-based approximations. However, the results do not change when using other samples (results not tabulated).

5.3 Comparing methods for predictive variances

Next, we compare the accuracy of the different approximations for predictive variances introduced in Section 3.2 using simulated data with $n = n_p = 100'000$ training and test points and a total of $m + m_p = 10'000$ group levels. The response variable follows a Gaussian likelihood, and we calculate the RMSE of the predictive variances compared to the “exact” Cholesky-based results. We also measure the runtime for prediction, which includes the calculation of the latent predictive means and variances. Predictive distributions are calculated at the true covariance parameters.

Figure 3 shows the RMSE versus the wall-clock time for different numbers of random vectors s for the stochastic methods and different ranks k for the Lanczos-based approximation. For the former, we average the results over 100 independent repetitions for every s and add whiskers to the plot representing confidence intervals for the RMSE obtained as $\pm 2 \times$ standard errors, but the corresponding whiskers are not visible since they are very small. By far the most accurate predictive variances for a given runtime are obtained with the simulation-based Algorithm 1. For instance, for $s = 200$, predictive variances are very accurate with an RMSE of approximately 2.6×10^{-4} , and the runtime is more than 100 times faster compared to Cholesky-based calculations. Algorithm 2 achieves the second highest prediction accuracy for a given runtime, and Algorithm 3 is considerably slower and less accurate. Finally, Lanczos-based approximations are very inaccurate and the RMSE decreases only very slowly with increasing rank k .

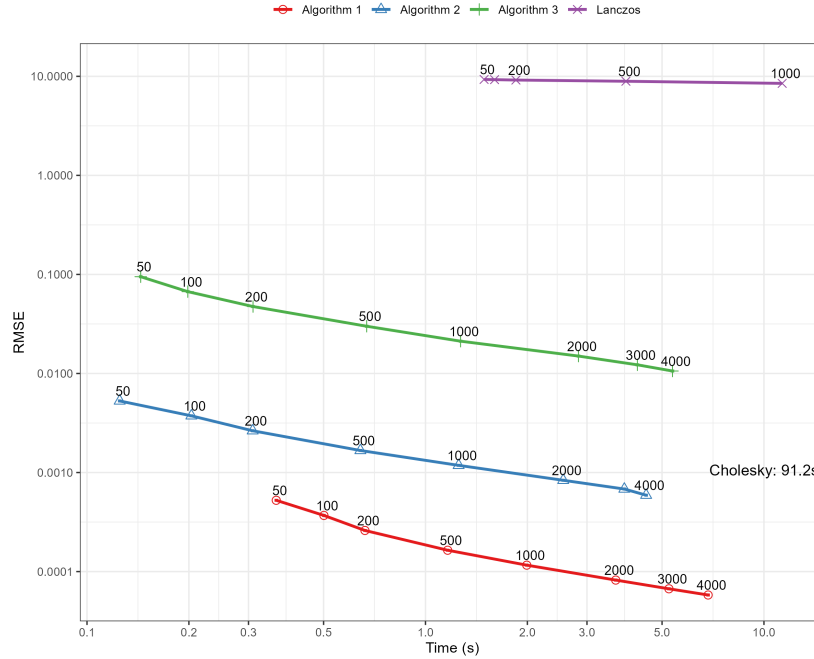


Figure 3: Comparison of different methods for predictive variances. The number of random vectors s and the Lanczos rank k are annotated in the plot.

5.4 Accuracy of parameter estimation and predictive distributions

In the following, we analyze the properties of the variance parameter and linear regression coefficient estimators and the accuracy of predictive distributions for Gaussian and Bernoulli likelihoods. We set the total number of group levels to $m + m_p = 4'000$ and simulate $n = n_p = 40'000$ training and test points. This is roughly the largest number of group levels such that we can run calculations with the `glmmTMB` and `lme4` packages in a reasonable amount of time. We perform 100 simulation repetitions, and prediction is done using estimated parameters. For Bernoulli likelihoods, repeating the estimation

100 times with `lme4` leads to very long runtimes; see also Section 5.5. Therefore, we do not report estimates and prediction accuracy for this case.

Figure 4 visualized the estimates for the variance parameters. The RMSE and bias of the variance and coefficient estimators are additionally reported in Appendix A.9 in Tables 2 and 3 for Gaussian and Bernoulli likelihoods, respectively. We observe virtually no differences among the estimates obtained using Krylov subspace methods and Cholesky-based computations with the `GPBoost`, `lme4`, and `glmmTMB` packages. Note that the variance parameter estimators for Bernoulli likelihoods are slightly downward biased due to the Laplace approximation and the moderate sample size.

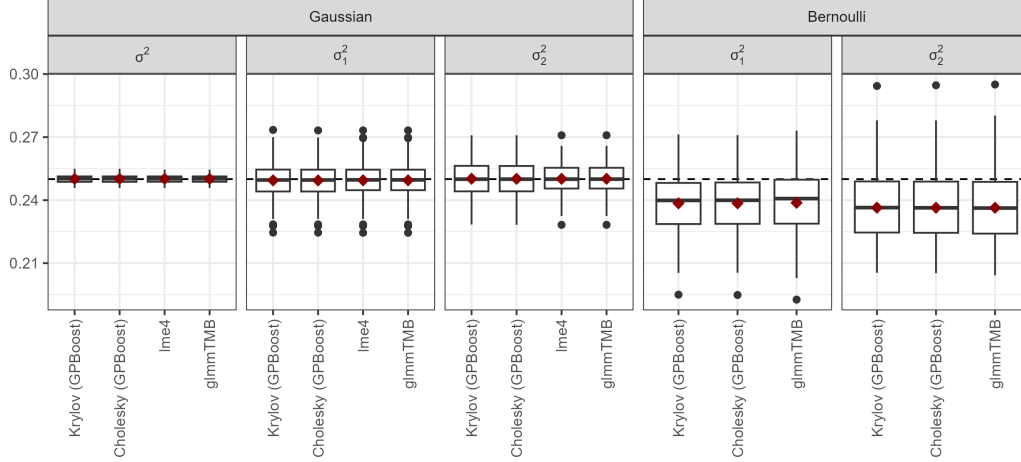


Figure 4: Estimated variance parameters. The red rhombi represent means. The dashed lines indicate the true values. For the Bernoulli likelihood the estimates for `lme4` are not computed due to excessively long runtimes.

Next, Figure 5 shows the RMSE for predictive means and the log score for predictive distributions. The average RMSE and the average log score with the corresponding standard errors are reported in Appendix A.9 in Tables 4 and 5 for Gaussian and Bernoulli likelihoods, respectively. Log scores are only reported for Krylov subspace methods and Cholesky-based computations from the `GPBoost` package since the calculation of predictive variances is not supported for `lme4` and leads to very long runtimes for `glmmTMB`. We observe that the predictions obtained with the Cholesky decomposition and the Krylov subspace methods have virtually the same accuracy in terms of both the RMSE and the log score.

5.5 Runtime comparison

In this subsection, we compare the runtime for parameter estimation when using Krylov subspace methods and Cholesky-based calculations with the `GPBoost`, `lme4`, and `glmmTMB` packages. For this, we consider different dimensions of the random effects ranging from $m = 1'000$ up to $m = 1'000'000$ and $n = 10m$ using the same setting as described in Section 5.1. Figure 6 shows the wall-clock time in seconds versus the total number of random effects m . Krylov subspace methods achieve the fastest runtime for all m . For instance, for $m = 20'000$ and a Gaussian likelihood, Krylov subspace methods are approximately three orders of magnitudes faster than Cholesky-based computations when using the `GPBoost` package. For a Gaussian likelihood, `glmmTMB` is approximately four orders of magnitudes slower than the Krylov subspace methods implemented in `GPBoost`, and `lme4` is approximately four orders of magnitudes slower than the Krylov subspace methods for a Bernoulli likelihood. In general, estimation takes the longest with `glmmTMB` for Gaussian likelihoods, and for Bernoulli likelihoods, estimation takes the longest with `lme4`.

In Figure 12 in Appendix A.9, we additionally compare the runtime for parameter estimation for an unbalanced random effects design with $m_2 = \frac{m_1}{2}$. Cholesky-based computations are faster compared to the balanced design due to the increased sparsity in $Z^T W Z$, but Krylov subspace methods again clearly achieve the fastest runtime for all m . For instance, they are three orders of magnitude faster

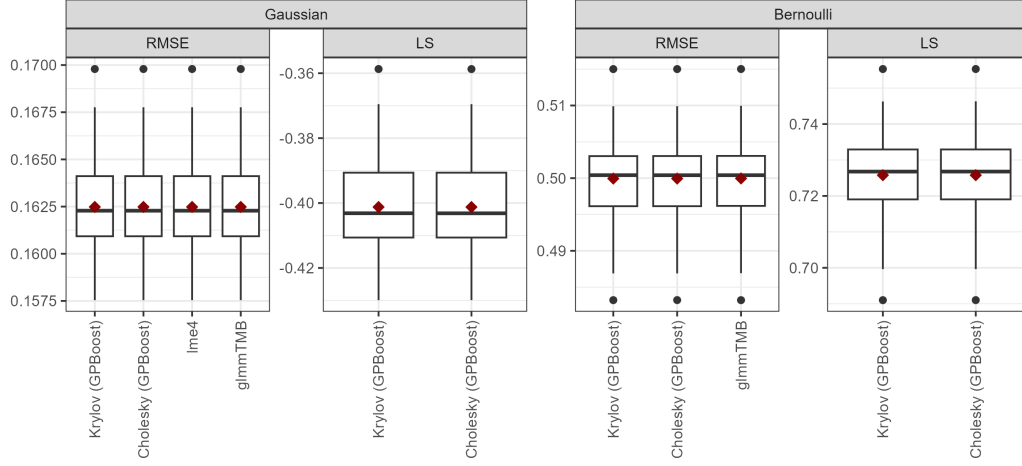


Figure 5: RMSE for predictive means and log score (LS) for probabilistic predictions for Gaussian and Bernoulli likelihoods.

than Cholesky-based computations using **GPBoost** for $m = 50'000$ and a Gaussian likelihood. Note that it would also be interesting to perform a runtime comparison for calculating log-marginal likelihoods as this would eliminate the impact of using different optimizers across different libraries, but the **lme4** and **glmmTMB** packages do not support the explicit calculation of marginal likelihoods. However, ‘Krylov (GPBoost)’ and ‘Cholesky (GPBoost)’ differ only in the use of Krylov subspace methods vs. Cholesky-based computations, and this comparison therefore clearly demonstrates the speed-up with Krylov subspace methods.

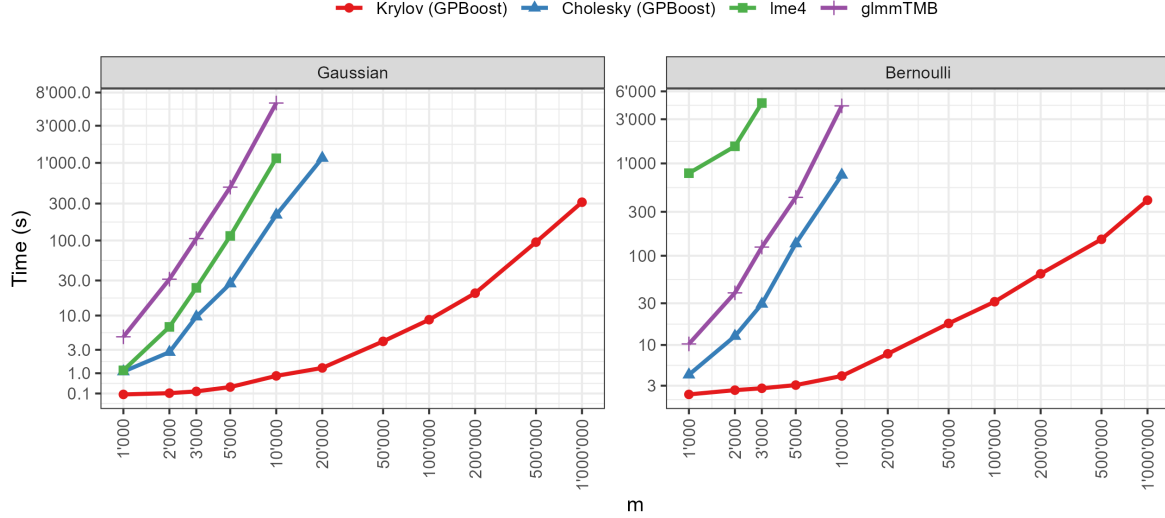


Figure 6: Average wall clock times (s) for parameter estimation and different m . Simulated data follows either a Gaussian or a Bernoulli likelihood.

6 Real-world applications

In the following, we conduct experiments on five real-world data sets with high-dimensional crossed random effects analyzing the runtime and accuracy for parameter estimation when using GLMMs. We compare the proposed Krylov subspace methods with Cholesky-based calculations from the **GPBoost**, **lme4**, and **glmmTMB** packages, using the same model and computational settings as described in Section

5.1. We use the ZIC preconditioner for the regression data sets and the SSOR preconditioner for the classification data sets.

6.1 Data sets

We consider three regression and two classification data sets. Table 1 gives an overview of the data sets reporting the sample size, the number of predictor variables, the categorical variables modeled using random effects including the number of group levels m_j , and the total number of non-zero entries in $Z^T Z$. In Figure 13 in Appendix A.10, we additionally visualize the non-zero entries of the matrix $Z^T Z$ for the different data sets. Note that the black areas in the plots should not hide the fact that the high-dimensional matrices are sparse, which can be seen when the number of nonzero entries is set in relation to the matrix dimensions. The data sets ‘upselling’ (‘KDDCup09_upselling’) and ‘employee_access’ (‘Amazon_employee_access’) have previously been used by Pargent et al. [2022]. For more information on the ‘instEval’ and ‘cars’ data sets, we refer to Simchoni and Rosset [2023], and the data set ‘building_permits’ (‘chicago_building_permits’) has been used by Reyes [2019]. In general, an extra category is added for missing values in categorical variables and numeric predictor variables are simply imputed using the mean.

	data set	n	p	K	y	%-class	Cat. var.	m_j	$\text{nzz}(Z^T Z)$
Regression	cars	97'729	66	2	$\log(\text{price})$		model_id	15'226	185'807
							location_id	12'235	
	building_permits	527'168	6	3	$\log(\text{cost})$		contact_name	98'362	2'544'893
							latitude	206'197	
							longitude	206'170	
Classification	instEval	73'421	22	2	teacher rating		student	2'972	150'942
							teacher	1'128	
	employee_access	32'769	0	9	approval	0.94	resource	7'518	469'262
							manager	4'243	
							role_cat1	128	
							role_cat2	177	
							role_dep.	449	
							role_title	343	
							role_descr.	2'358	
							role_family	67	
							role_code	343	
	upselling	50'000	34	4	up-selling	0.07	Var216	2'016	454'852
							Var217	13'991	
							Var198	4'291	
							Var199	5'074	

Table 1: Summary of real-world data sets. n is the number of samples, p is the number of predictor variables, K is the number of categorical variables modeled with random effects, y describes the response variable, ‘%-class’ is the frequency of the ‘1’ response variables for the classification data sets, ‘Cat. var.’ describes the categorical variables modeled with random effects, m_j is the number of group levels, and $\text{nzz}(Z^T Z)$ is the number of non-zero entries in the matrix $Z^T Z$.

6.2 Results

Figure 7 shows the estimation runtimes for the different data sets. In Appendix A.10, we additionally report the wall-clock time, the log-marginal likelihood at the optimum, and the estimated parameters. Parameter estimation crashes when using the `lme4` and `glmmTMB` packages on the ‘upselling’ data set. We have additionally tried modeling only the two variables Var216 and Var217 as random effects but still observed crashes on the ‘upselling’ data set. For the ‘employee_access’ data set, we have also tried modeling the low-cardinality categorical variables such as ‘role.family’ and ‘role_cat1’ as dummy-coded fixed effects instead of random effects, but `glmmTMB` and `lme4` crash when doing this. In Figure 8, we

report the average differences in estimation runtime relative to the fastest model over the four data sets for which `glmmTMB` and `lme4` do not crash.

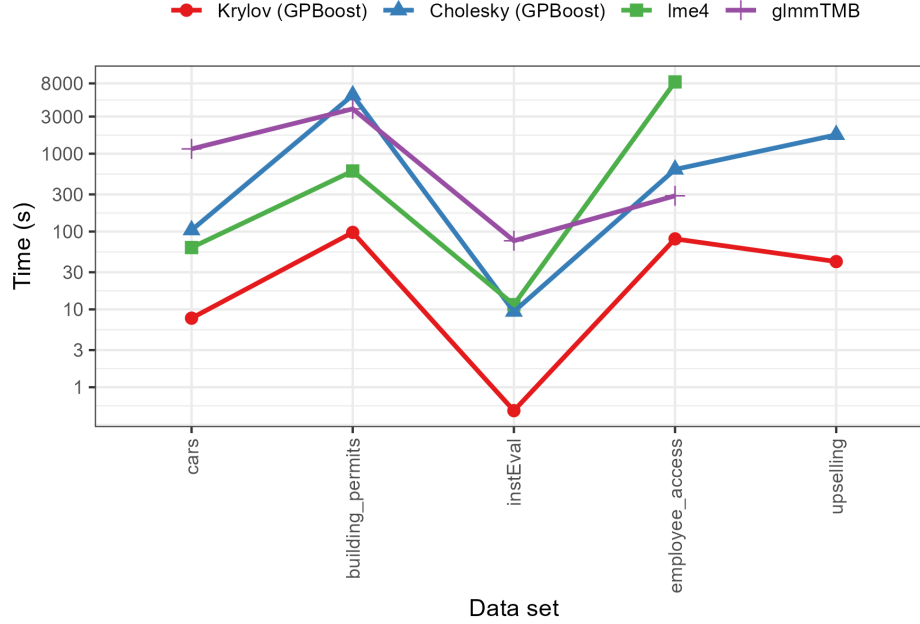


Figure 7: Runtimes for estimation on different real-world data sets for different models.

The results show that Krylov subspace methods clearly have the fastest runtime on all real-world data sets. Compared to Cholesky-based calculations using the `GPBoost` package, the average speed-up with Krylov subspace methods is more than a factor of 20. On the high-dimensional ‘building-permits’ data set, parameter estimation with Krylov subspace methods is over 57 times faster compared to Cholesky-based calculations in `GPBoost`. Moreover, estimation is, on average, more than 30 and 80 times slower when using `lme4` and `glmmTMB`, respectively, compared to Krylov subspace-based methods. On average, the estimation time of `lme4` is the second smallest for the three regression data sets. However, as observed in experiments with simulated data, `lme4` is very slow on classification data and can crash, e.g., on the ‘upselling’ data set. `glmmTMB` has overall the longest runtime. Concerning the parameter estimates reported in Tables 8 and 7 in Appendix A.10, we find that all methods and packages yield essentially the same estimates except for `lme4` on the ‘building-permits’ and ‘employee-access’ data sets. In summary, our novel Krylov subspace-based methods are substantially faster than Cholesky-based calculations and numerically more stable than existing software libraries for GLMMs.

7 Conclusion

We present Krylov subspace methods for mixed effects models with high-dimensional crossed random effects. We analyze several preconditioners, derive novel theoretical results, and introduce different methods for accurately approximating predictive variances. In experiments, we find that our methods are faster and more stable than Cholesky-based calculations and other state-of-the-art software implementations for GLMMs. In addition, we provide theoretical and empirical results showing that the symmetric successive over-relaxation (SSOR) preconditioner is superior compared to the popular diagonal preconditioner for both the CG and the SLQ methods. Potential directions for future research include analyzing alternative approximations for log-determinants, a systematic comparison under which situations the ZIC or the SSOR preconditioners are preferred, and the development of novel preconditioners.

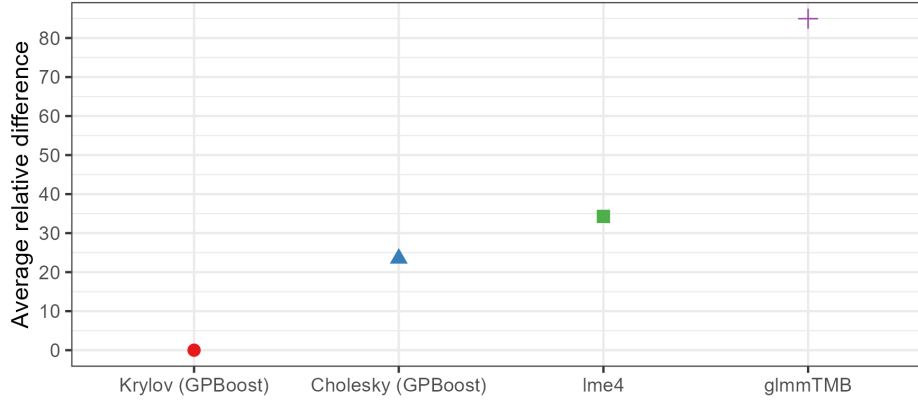


Figure 8: Average relative difference in runtime to the fastest model over all real-world data sets except for the data set ‘upselling’ where `lme4` and `glmmTMB` crash.

Acknowledgments

This research was partially supported by the Swiss Innovation Agency - Innosuisse (grant number ‘55463.1 IP-ICT’).

References

- B. Avanzi, G. Taylor, M. Wang, and B. Wong. Machine learning with high-cardinality categorical features in actuarial applications. *ASTIN Bulletin: The Journal of the IAA*, 54(2):213–238, 2024.
- C. Bekas, E. Kokiopoulou, and Y. Saad. An estimator for the diagonal of a matrix. *Applied numerical mathematics*, 57(11-12):1214–1229, 2007.
- R. Bellio, S. Ghosh, A. B. Owen, and C. Varin. Consistent and scalable composite likelihood estimation of probit models with crossed random effects. *arXiv preprint arXiv:2308.15681*, 2023.
- R. Border and S. Becker. Stochastic lanczos estimation of genomic variance components for linear mixed-effects models. *BMC bioinformatics*, 20:1–16, 2019.
- G. Brito, I. Dumitriu, and K. D. Harris. Spectral gap in random bipartite biregular graphs and applications. *Combinatorics, Probability and Computing*, 31(2):229–267, 2022.
- J. Cheng, C. Maltecca, P. M. VanRaden, J. R. O’Connell, L. Ma, and J. Jiang. Slemm: million-scale genomic predictions with window-based snp weighting. *Bioinformatics*, 39(3):btad127, 2023.
- F. R. Chung. *Spectral graph theory*, volume 92. American Mathematical Soc., 1997.
- K. Dong, D. Eriksson, H. Nickisch, D. Bindel, and A. G. Wilson. Scalable log determinants for gaussian process kernel learning. *Advances in Neural Information Processing Systems*, 30, 2017.
- W. Fu and J. S. Simonoff. Unbiased regression trees for longitudinal and clustered data. *Computational Statistics & Data Analysis*, 88:53–74, 2015.
- K. Gao and A. Owen. Efficient moment calculations for variance components in large unbalanced crossed random effects models. *Electronic Journal of Statistics*, 11:1235–1296, 2017.
- K. Gao and A. B. Owen. Estimation and inference for very large linear mixed effects models. *Statistica Sinica*, 30(4):1741–1771, 2020.
- J. Gardner, G. Pleiss, K. Q. Weinberger, D. Bindel, and A. G. Wilson. Gpytorch: Blackbox matrix-matrix gaussian process inference with gpu acceleration. *Advances in neural information processing systems*, 31, 2018.

- D. J. Garrick, B. L. Golden, and D. P. Garrick. Alternative implementations of preconditioned conjugate gradient algorithms for solving mixed model equations. page 250–253, Armidale, 2019. Association for the Advancement of Animal Breeding and Genetics.
- S. Ghosh, T. Hastie, and A. B. Owen. Backfitting for large scale crossed random effects regressions. *The Annals of Statistics*, 50(1):560–583, 2022a.
- S. Ghosh, T. Hastie, and A. B. Owen. Scalable logistic regression with crossed random effects. *Electronic Journal of Statistics*, 16(2):4604–4635, 2022b.
- G. H. Golub and C. F. Van Loan. *Matrix computations*. JHU press, 2013.
- M. Goplerud, O. Papaspiliopoulos, and G. Zanella. Partially factorized variational inference for high-dimensional mixed models. *Biometrika*, page asae067, 2025.
- T. Gyger, R. Furrer, and F. Sigrist. Iterative methods for full-scale gaussian process approximations for large spatial data. *arXiv preprint arXiv:2405.14492*, 2024.
- A. Hajjem, F. Bellavance, and D. Larocque. Mixed effects regression trees for clustered data. *Statistics & probability letters*, 81(4):451–459, 2011.
- A. Hajjem, F. Bellavance, and D. Larocque. Mixed-effects random forest for clustered data. *Journal of Statistical Computation and Simulation*, 84(6):1313–1328, 2014.
- H. Harbrecht, M. Peters, and R. Schneider. On the low-rank approximation by the pivoted cholesky decomposition. *Applied numerical mathematics*, 62(4):428–440, 2012.
- R. A. Horn and C. R. Johnson. *Matrix analysis*. Cambridge university press, 2012.
- S. Kim, R. Pasupathy, and S. G. Henderson. A guide to sample average approximation. *Handbook of simulation optimization*, pages 207–243, 2015.
- P. Kündig and F. Sigrist. Iterative methods for vecchia-laplace approximations for latent gaussian process models. *Journal of the American Statistical Association*, pages 1–14, 2024.
- N. M. Laird and J. H. Ware. Random-effects models for longitudinal data. *Biometrics*, pages 963–974, 1982.
- A. Nishimura and M. A. Suchard. Prior-preconditioned conjugate gradient method for accelerated gibbs sampling in “large n, large p” bayesian sparse regression. *Journal of the American Statistical Association*, pages 1–14, 2022.
- A. Pandolfi, O. Papaspiliopoulos, and G. Zanella. Conjugate gradient methods for high-dimensional glmms. *arXiv preprint arXiv:2411.04729*, 2024.
- O. Papaspiliopoulos, G. O. Roberts, and G. Zanella. Scalable inference for crossed random effects models. *Biometrika*, 107(1):25–40, 2020.
- O. Papaspiliopoulos, T. Stumpf-Fétizon, and G. Zanella. Scalable bayesian computation for crossed and nested hierarchical models. *Electronic Journal of Statistics*, 17(2):3575–3612, 2023.
- F. Pargent, F. Pfisterer, J. Thomas, and B. Bischl. Regularized target encoding outperforms traditional methods in supervised machine learning with high cardinality features. *Computational Statistics*, 37(5):2671–2692, 2022.
- J. C. Pinheiro and D. M. Bates. Linear mixed-effects models: basic concepts and examples. *Mixed-effects models in S and S-Plus*, pages 3–56, 2000.
- G. Pleiss, J. Gardner, K. Weinberger, and A. G. Wilson. Constant-time predictive distributions for gaussian processes. In *International Conference on Machine Learning*, pages 4114–4123. PMLR, 2018.
- P. C. Reyes. *Statistical learning with high-cardinality string categorical variables*. PhD thesis, Université Paris-Saclay, 2019.

- Y. Saad. *Iterative methods for sparse linear systems*. SIAM, 2003.
- J. Scott and M. Tuma. On positive semidefinite modification schemes for incomplete cholesky factorization. *SIAM Journal on Scientific computing*, 36(2):A609–A633, 2014.
- R. J. Sela and J. S. Simonoff. Re-em trees: a data mining approach for longitudinal and clustered data. *Machine learning*, 86:169–207, 2012.
- F. Sigrist. Gaussian process boosting. *Journal of Machine Learning Research*, 23(232):1–46, 2022.
- F. Sigrist. Latent gaussian model boosting. *IEEE Transactions on Pattern Analysis and Machine Intelligence*, 45(2):1894–1905, 2023a.
- F. Sigrist. A comparison of machine learning methods for data with high-cardinality categorical variables. *arXiv preprint arXiv:2307.02071*, 2023b.
- G. Simchoni and S. Rosset. Using random effects to account for high-cardinality categorical features and repeated measures in deep neural networks. *Advances in Neural Information Processing Systems*, 34:25111–25122, 2021.
- G. Simchoni and S. Rosset. Integrating random effects in deep neural networks. *Journal of Machine Learning Research*, 24(156):1–57, 2023.
- I. Strandén and M. Lidauer. Solving large mixed linear models using preconditioned conjugate gradient iteration. *Journal of Dairy Science*, 82(12):2779–2787, 1999.
- I. Strandén and M. Lidauer. Parallel computing applied to breeding value estimation in dairy cattle. *Journal of dairy science*, 84(1):276–285, 2001.
- M. Taskinen, E. A. Mäntysaari, and I. Strandén. Single-step snp-blup with on-the-fly imputed genotypes and residual polygenic effects. *Genetics Selection Evolution*, 49:1–15, 2017.
- S. Tsuruta, I. Misztal, and I. Strandén. Use of the preconditioned conjugate gradient algorithm as a generic solver for mixed-model equations in animal breeding applications. *Journal of animal science*, 79(5):1166–1172, 2001.
- S. Ubaru, J. Chen, and Y. Saad. Fast estimation of $\text{tr}(\mathbf{f}(\mathbf{a}))$ via stochastic lanczos quadrature. *SIAM Journal on Matrix Analysis and Applications*, 38(4):1075–1099, 2017.
- A. Van der Sluis and H. A. van der Vorst. The rate of convergence of conjugate gradients. *Numerische Mathematik*, 48:543–560, 1986.
- H. A. Van der Vorst. *Iterative Krylov methods for large linear systems*. Number 13. Cambridge University Press, 2003.
- J. Vandenplas, H. Eding, M. P. Calus, and C. Vuik. Deflated preconditioned conjugate gradient method for solving single-step blup models efficiently. *Genetics Selection Evolution*, 50:1–17, 2018.
- J. Wenger, G. Pleiss, P. Hennig, J. Cunningham, and J. Gardner. Preconditioning for scalable gaussian process hyperparameter optimization. In *International Conference on Machine Learning*, pages 23751–23780. PMLR, 2022.
- C. K. Williams and C. E. Rasmussen. *Gaussian processes for machine learning*. MIT Press Cambridge, MA, 2006.
- K. Wu and H. Simon. Thick-restart lanczos method for large symmetric eigenvalue problems. *SIAM Journal on Matrix Analysis and Applications*, 22(2):602–616, 2000.
- L. Xu, N. Reid, and D. Kong. Gaussian variational approximation with composite likelihood for crossed random effect models. *arXiv preprint arXiv:2310.12485*, 2023.

A Appendix

A.1 Proofs of results in Section 4

We denote by $\sigma_{\min}(B) = \sigma_{\min(n_1, n_2)}(B) \leq \dots \leq \sigma_1(B) = \sigma_{\max}(B)$ the singular values of a matrix $B \in \mathbb{R}^{n_1 \times n_2}$, and by $\lambda_{\min}(A) = \lambda_m(A) \leq \dots \leq \lambda_1(A) = \lambda_{\max}(A)$ the eigenvalues of a symmetric matrix $A \in \mathbb{R}^{m \times m}$. Further, we denote by $D = \Sigma^{-1} + \text{diag}(Z^T W Z) \in \mathbb{R}^{m \times m}$, $\Delta = \text{diag}(Z^T W Z) \in \mathbb{R}^{m \times m}$, and $\Lambda = Z^T W Z - \text{diag}(Z^T W Z) \in \mathbb{R}^{m \times m}$.

We will use the following two lemmas for proofing Theorem 4.2.

Lemma A.1. *For any $B \in \mathbb{R}^{n_1 \times n_2}$ and $A = \begin{pmatrix} 0 & B^T \\ B & 0 \end{pmatrix} \in \mathbb{R}^{(n_1+n_2) \times (n_1+n_2)}$, the non-zero eigenvalues of A are equal to \pm the singular values of B , i.e.,*

$$\{\lambda_i(A); i = 1, \dots, 2 \min(n_1, n_2)\} = \{\pm \sigma_i(B); i = 1, \dots, \min(n_1, n_2)\}.$$

In particular, the largest singular value of B and the largest eigenvalue of A are equal, $\lambda_{\max}(A) = \sigma_{\max}(B)$. The same holds true for the second largest singular value and eigenvalue.

Proof of Lemma A.1. The eigenvalues of A are defined as solutions to

$$\det(A - \lambda I) = 0.$$

Since $A - \lambda I$ is a block matrix, we have

$$\det(A - \lambda I) = \det(\lambda^2 I - B^T B).$$

The eigenvalues of A are thus given by

$$\{\pm \sqrt{\lambda_i(B^T B)}; i = 1, \dots, \min(n_1, n_2)\} = \{\pm \sigma_i(B); i = 1, \dots, \min(n_1, n_2)\}.$$

□

Lemma A.2. *For any matrix $B \in \mathbb{R}^{n_1 \times n_2}$ and diagonal matrices $C_1^{n_1 \times n_1}$ and $C_2^{n_2 \times n_2}$, it holds that*

$$\sigma_{\max}(B) \min(|(C_1)_{ii}|) \min(|(C_2)_{jj}|) \leq \sigma_{\max}(C_1 B C_2) \leq \sigma_{\max}(B) \max(|(C_1)_{ii}|) \max(|(C_2)_{jj}|).$$

Proof of Lemma A.2.

$$\sigma_{\max}(C_1 B C_2) = \|C_1 B C_2\|_2 \leq \|C_1\|_2 \|B\|_2 \|C_2\|_2 = \sigma_{\max}(B) \max(|(C_1)_{ii}|) \max(|(C_2)_{jj}|).$$

Furthermore,

$$\sigma_{\max}(B) = \|B\|_2 = \|C_1^{-1} C_1 B C_2 C_2^{-1}\|_2 \leq \sigma_{\max}(C_1 B C_2) \frac{1}{\min(|(C_1)_{ii}|)} \frac{1}{\min(|(C_2)_{ii}|)}$$

which gives the first inequality. □

Proof of Theorem 4.2. For the SSOR preconditioner $P_{\text{SSOR}} = (L + D)D^{-1}(L + D)^T$, we have

$$L = \begin{pmatrix} 0 & 0 \\ Z_2^T W Z_1 & 0 \end{pmatrix}, \quad D = \begin{pmatrix} D_1 & 0 \\ 0 & D_2 \end{pmatrix}, \quad \Sigma^{-1} + Z^T W Z = \begin{pmatrix} D_1 & Z_1^T W Z_2 \\ Z_2^T W Z_1 & D_2 \end{pmatrix}.$$

It can easily be seen that

$$(D + L)^{-1} = \begin{pmatrix} D_1^{-1} & 0 \\ -D_2^{-1} Z_2^T W Z_1 D_1^{-1} & D_2^{-1} \end{pmatrix},$$

and (21) thus follows since

$$\begin{aligned} P_{\text{SSOR}}^{-1/2} (\Sigma^{-1} + Z^T W Z) P_{\text{SSOR}}^{-T/2} &= D^{1/2} (D + L)^{-1} (\Sigma^{-1} + Z^T W Z) (D + L)^{-T} D^{1/2} \\ &= I_m - \begin{pmatrix} 0 & 0 \\ 0 & D_2^{-1/2} Z_2^T W Z_1 D_1^{-1} Z_1^T W Z_2 D_2^{-1/2} \end{pmatrix}. \end{aligned} \quad (43)$$

Because $D_2^{-1/2} Z_2^T W Z_1 D_1^{-1} Z_1^T W Z_2 D_2^{-1/2}$ is a symmetric positive semi-definite matrix and using the fact that $\lambda_i(I_m + A) = 1 + \lambda_i(A)$ for any normal matrix A , we obtain (22).

Using Lemma A.1, we have

$$\begin{aligned}\sigma_{\max}(D_2^{-1/2} Z_2^T W Z_1 D_1^{-1/2}) &= \lambda_{\max} \begin{pmatrix} 0 & D_1^{-1/2} Z_1^T W Z_2 D_2^{-1/2} \\ D_2^{-1/2} Z_2^T W Z_1 D_1^{-1/2} & 0 \end{pmatrix} \\ &= \lambda_{\max}(D^{-1/2} \Lambda D^{-1/2}) \\ &= \lambda_{\max}(D^{-1/2} \Delta^{1/2} \Delta^{-1/2} \Lambda \Delta^{-1/2} \Delta^{1/2} D^{-1/2}).\end{aligned}$$

Note that $\Delta^{-1/2} \Lambda \Delta^{-1/2}$ is a normalized adjacency matrix of a bipartite weighted graph. Its largest eigenvalues is thus 1 [Chung, 1997]. By Lemma A.2, or Ostrowski's theorem [Horn and Johnson, 2012], it follows that

$$\min((D^{-1} \Delta)_{ii}) \leq \sigma_{\max}(D_2^{-1/2} Z_2^T W Z_1 D_1^{-1/2}) \leq \max((D^{-1} \Delta)_{ii}).$$

Since $D^{-1} \Delta = \text{diag} \left(\frac{1}{\sum_{ii}^{-1} \Delta_{ii}^{-1} + 1} \right)$ and

$$\lambda_i(D_2^{-1/2} Z_2^T W Z_1 D_1^{-1} Z_1^T W Z_2 D_2^{-1/2}) = \sigma_i(D_2^{-1/2} Z_2^T W Z_1 D_1^{-1/2})^2, \quad 1 \leq i \leq \min(m_1, m_2), \quad (44)$$

we have

$$\frac{1}{(\max(\sum_{ii}^{-1} \Delta_{ii}^{-1}) + 1)^2} \leq \lambda_{\max}(D_2^{-1/2} Z_2^T W Z_1 D_1^{-1} Z_1^T W Z_2 D_2^{-1/2}) \leq \frac{1}{(\min(\sum_{ii}^{-1} \Delta_{ii}^{-1}) + 1)^2},$$

from which follows (23).

Furthermore, since

$$\sigma_{\max}(Z_2^T W Z_1) = \lambda_{\max} \begin{pmatrix} 0 & Z_1^T W Z_2 \\ Z_2^T W Z_1 & 0 \end{pmatrix} = \lambda_{\max}(\Lambda) = \lambda_{\max}(\Delta^{1/2} \Delta^{-1/2} \Lambda \Delta^{-1/2} \Delta^{1/2}).$$

and applying Lemma A.2, we obtain

$$\min(\Delta_{ii}) \leq \sigma_{\max}(Z_2^T W Z_1) \leq \max(\Delta_{ii}).$$

By again using Lemma A.2, we obtain

$$\min((D_1^{-1/2})_{ii}) \min((D_2^{-1/2})_{ii}) \min(\Delta_{ii}) \leq \sigma_{\max}(D_2^{-1/2} Z_2^T W Z_1 D_1^{-1/2}) \leq \max((D_1^{-1/2})_{ii}) \max((D_2^{-1/2})_{ii}) \max(\Delta_{ii})$$

and

$$\min((D_1^{-1})_{ii}) \min((D_2^{-1})_{ii}) \min(\Delta_{ii}^2) \leq \lambda_{\max}(D_2^{-1/2} Z_2^T W Z_1 D_1^{-1} Z_1^T W Z_2 D_2^{-1/2}) \leq \max((D_1^{-1})_{ii}) \max((D_2^{-1})_{ii}) \max(\Delta_{ii}^2)$$

which gives the second set of inequalities for $\lambda_{\min}^{\text{SSOR}}$ in (24). \square

Proof of Theorem 4.3. Similarly as in the proof of Theorem 4.2, we can apply Lemma A.1 and obtain

$$\begin{aligned}\sigma_2 \left(\frac{1}{\sigma^2} D_2^{-1/2} Z_2^T Z_1 D_1^{-1/2} \right) &= \lambda_2 \left(\frac{1}{\sigma^2} D^{-1/2} \begin{pmatrix} 0 & Z_1^T Z_2 \\ Z_2^T Z_1 & 0 \end{pmatrix} D^{-1/2} \right) \\ &= \lambda_2 \left(\begin{pmatrix} 0 & Z_1^T Z_2 \\ Z_2^T Z_1 & 0 \end{pmatrix} \frac{1}{\sqrt{\sigma^2/\sigma_1^2 + d_1}} \frac{1}{\sqrt{\sigma^2/\sigma_2^2 + d_2}} \right),\end{aligned} \quad (45)$$

where we have used

$$\sigma^{-1} D^{-1/2} = \text{diag} \left(\frac{1}{\sqrt{\sigma^2/\sigma_1^2 + d_1}}, \dots, \frac{1}{\sqrt{\sigma^2/\sigma_1^2 + d_1}}, \frac{1}{\sqrt{\sigma^2/\sigma_2^2 + d_2}}, \dots, \frac{1}{\sqrt{\sigma^2/\sigma_2^2 + d_2}} \right).$$

Applying Theorem 3.2 of Brito et al. [2022] to $\lambda_2 \begin{pmatrix} 0 & Z_1^T Z_2 \\ Z_2^T Z_1 & 0 \end{pmatrix}$ then shows that

$$\begin{aligned}\sigma_2 \left(\frac{1}{\sigma^2} D_2^{-1/2} Z_2^T Z_1 D_1^{-1/2} \right) &\leq \frac{\sqrt{d_1 - 1} + \sqrt{d_2 - 1}}{\sqrt{\sigma^2/\sigma_1^2 + d_1} \sqrt{\sigma^2/\sigma_2^2 + d_2}} + \epsilon'_m \\ &\leq \frac{1}{\sqrt{d_1}} + \frac{1}{\sqrt{d_2}} + \epsilon'_m\end{aligned}$$

asymptotically almost surely with $\epsilon'_m \rightarrow 0$ as $m \rightarrow \infty$. Using (43) and (44) proofs (27). (28) follows directly from (27). \square

Proof of Theorem 4.4. Consider the vectors

$$v_k = D^{1/2} \left(\frac{1}{k} 1_{m_1}^T, \dots, \frac{1}{k} 1_{m_k}^T, -1_{m_{k+1}}^T, 0, \dots, 0 \right)^T \in \mathbb{R}^m, \quad k = 1, \dots, K-1,$$

where 1_{m_k} denotes a vectors of 1's of length m_k . We have $D^{-1/2} Z^T W Z D^{-1/2} v_k = 0$, and the vectors v_k are linearly independent. Since $D^{-1/2} Z^T W Z D^{-1/2}$ is positive semi-definite, this shows that the $K-1$ smallest eigenvalues of $D^{-1/2} Z^T W Z D^{-1/2}$ are zero. Applying Weyl's inequality [Horn and Johnson, 2012] to $P_{\text{Diag}}^{-1/2} (\Sigma^{-1} + Z^T W Z) P_{\text{Diag}}^{-T/2} = D^{-1/2} \Sigma^{-1} D^{-1/2} + D^{-1/2} Z^T W Z D^{-1/2}$ gives

$$\lambda_{\min}(D^{-1/2} \Sigma^{-1} D^{-1/2}) \leq \lambda_{m+1-k}(P_{\text{Diag}}^{-1/2} (\Sigma^{-1} + Z^T W Z) P_{\text{Diag}}^{-T/2}) \leq \lambda_{\max}(D^{-1/2} \Sigma^{-1} D^{-1/2})$$

for $k = 1, \dots, K-1$, which proofs (30).

Similarly as in the proof of Theorem 4.2, we can show, for general K , that

$$(K-1) \min((D^{-1} \Delta)_{ii}) \leq \lambda_{\max}(D^{-1/2} \Lambda D^{-1/2}) \leq (K-1) \max((D^{-1} \Delta)_{ii}). \quad (46)$$

For doing this, we first note that Λ is an adjacency matrix of a connected, K -partite weighted graph. Moreover,

$$\begin{aligned} \sum_{j=1}^m \Lambda_{ij} &= \sum_{k=1, k \neq \tilde{k}(i)}^K \sum_{j=1}^{m_k} (Z_{\tilde{k}(i)}^T W Z_k)_{ij} \\ &= \sum_{k=1, k \neq \tilde{k}(i)}^K \sum_{j=1}^{m_k} \sum_{l=1}^n W_{ll} (Z_{\tilde{k}(i)})_{li} (Z_k)_{lj} \\ &= \sum_{k=1, k \neq \tilde{k}(i)}^K \sum_{l=1}^n W_{ll} (Z_{\tilde{k}(i)})_{li} \\ &= \sum_{k=1, k \neq \tilde{k}(i)}^K \Delta_{ii} = (K-1) \Delta_{ii} \end{aligned}$$

where $\tilde{k}(i) = k$ if $i \in \{\sum_{k'=0}^{k-1} m_{k'} + 1, \dots, \sum_{k'=0}^k m_{k'}\}$ with the convention $m_0 = 0$. This shows that $\frac{1}{K-1} \Delta^{-1/2} \Lambda \Delta^{-1/2}$ is a normalized adjacency matrix of a connected, K -partite weighted graph whose largest eigenvalue is 1. Using

$$\lambda_{\max}(D^{-1/2} \Lambda D^{-1/2}) = (K-1) \lambda_{\max}(D^{-1/2} \Delta^{1/2} \frac{1}{K-1} \Delta^{-1/2} \Lambda \Delta^{-1/2} \Delta^{1/2} D^{-1/2})$$

gives (46), which together with

$$P_{\text{Diag}}^{-1/2} (\Sigma^{-1} + Z^T W Z) P_{\text{Diag}}^{-T/2} = I_m + D^{-1/2} \Lambda D^{-1/2} \quad (47)$$

proofs the statement in (29). \square

Proof of Theorem 4.5. First, (31) and (32) follow directly from (29) and (30).

For (33), note that

$$\begin{aligned} D^{-1/2} \Delta^{1/2} &= \text{diag} \left(\frac{1}{\Sigma_{ii}^{-1} \Delta_{ii}^{-1} + 1} \right)^{1/2} \\ &= \text{diag} \left(\frac{1}{\sqrt{\frac{\sigma^2}{\sigma_1^2 d_1} + 1}}, \dots, \frac{1}{\sqrt{\frac{\sigma^2}{\sigma_1^2 d_1} + 1}}, \frac{1}{\sqrt{\frac{\sigma^2}{\sigma_2^2 d_2} + 1}}, \dots, \frac{1}{\sqrt{\frac{\sigma^2}{\sigma_2^2 d_2} + 1}} \right), \end{aligned}$$

which implies

$$D^{-1/2} \Delta^{1/2} \Delta^{-1/2} \Lambda \Delta^{-1/2} \Delta^{1/2} D^{-1/2} = \frac{1}{\sqrt{\frac{\sigma^2}{\sigma_1^2 d_1} + 1}} \frac{1}{\sqrt{\frac{\sigma^2}{\sigma_2^2 d_2} + 1}} \Delta^{-1/2} \Lambda \Delta^{-1/2}. \quad (48)$$

Using $\lambda_{\max}(\Delta^{-1/2} \Lambda \Delta^{-1/2}) = K - 1$, see the proof of Theorem 4.4, then gives

$$\begin{aligned} \lambda_{\max}(D^{-1/2} \Lambda D^{-1/2}) &= \lambda_{\max}(D^{-1/2} \Delta^{1/2} \Delta^{-1/2} \Lambda \Delta^{-1/2} \Delta^{1/2} D^{-1/2}) \\ &= \frac{K - 1}{\sqrt{\frac{\sigma^2}{\sigma_1^2 d_1} + 1} \sqrt{\frac{\sigma^2}{\sigma_2^2 d_2} + 1}}. \end{aligned}$$

This and (47) proof (33).

By analogous arguments, again using (48) and $\lambda_{\min}(\Delta^{-1/2} \Lambda \Delta^{-1/2}) = -1$ due to Lemma A.1, we have

$$\lambda_{\min}(D^{-1/2} \Lambda D^{-1/2}) = -\frac{1}{\sqrt{\frac{\sigma^2}{\sigma_1^2 d_1} + 1}} \frac{1}{\sqrt{\frac{\sigma^2}{\sigma_2^2 d_2} + 1}},$$

which gives (34). \square

Proof of Theorem 4.6. We have

$$\Sigma^{-1} + Z^T W Z = \Sigma^{-1} + \Delta^{1/2} (I_m + \Delta^{-1/2} \Lambda \Delta^{-1/2}) \Delta^{1/2}.$$

Applying Weyl's inequality [Horn and Johnson, 2012], Ostrowski's theorem [Horn and Johnson, 2012], and the fact that the largest eigenvalue of $\Delta^{-1/2} \Lambda \Delta^{-1/2}$ is $K - 1$, see the proof of Theorem 4.4, we obtain (35). (36) is shown analogously as (30) in the proof of Theorem 4.4. \square

Proof of Theorem 4.7. First, (37) follows directly from Corollary 4.1 and Theorem 4.5. Next, by Corollary 4.1, we have

$$\lambda_{\min}^{\text{SSOR}} = 1 - \frac{\sigma_1^2 d}{\sigma^2 + \sigma_1^2 d} \frac{\sigma_2^2 d}{\sigma^2 + \sigma_2^2 d} = \frac{(\sigma^2)^2 + \sigma^2(\sigma_1^2 + \sigma_2^2)d}{(\sigma^2)^2 + \sigma^2(\sigma_1^2 + \sigma_2^2)d + \sigma_1^2 \sigma_2^2 d^2}$$

and thus

$$\frac{\lambda_{\max}^{\text{SSOR}}}{\lambda_{\min}^{\text{SSOR}}} = \frac{(\sigma^2)^2/d + \sigma^2(\sigma_1^2 + \sigma_2^2) + \sigma_1^2 \sigma_2^2 d}{(\sigma^2)^2/d + \sigma^2(\sigma_1^2 + \sigma_2^2)},$$

and (38) follows. By Theorem 4.5, we have

$$\frac{\lambda_{\max}^{\text{Diag}}}{\lambda_{\min}^{\text{Diag}}} = \frac{\left(1 + \frac{1}{\sqrt{\left(\frac{\sigma^2}{\sigma_1^2 d} + 1\right) \left(\frac{\sigma^2}{\sigma_2^2 d} + 1\right)}}\right)}{\left(1 - \frac{1}{\sqrt{\left(\frac{\sigma^2}{\sigma_1^2 d} + 1\right) \left(\frac{\sigma^2}{\sigma_2^2 d} + 1\right)}}\right)} = \frac{\sqrt{\left(\frac{\sigma^2}{\sigma_1^2 d} + 1\right) \left(\frac{\sigma^2}{\sigma_2^2 d} + 1\right)} + 1}{\sqrt{\left(\frac{\sigma^2}{\sigma_1^2 d} + 1\right) \left(\frac{\sigma^2}{\sigma_2^2 d} + 1\right)} - 1}. \quad (49)$$

Using

$$\sqrt{\left(\frac{\sigma^2}{\sigma_1^2 d} + 1\right) \left(\frac{\sigma^2}{\sigma_2^2 d} + 1\right)} = 1 + \frac{1}{2} \left(\frac{\sigma^2}{\sigma_1^2 d} + \frac{\sigma^2}{\sigma_2^2 d}\right) + \mathcal{O}(d^{-2}),$$

one can show that $\frac{\lambda_{\max}^{\text{Diag}}}{\lambda_{\min}^{\text{Diag}}}$ has the linear asymptote in d given in (39). (40) follows from Theorem 4.6. \square

A.2 Effective condition number for the diagonal preconditioner and proof of Theorem 4.8

Theorem A.1. *If $K = 2$, the likelihood is Gaussian, and $\begin{pmatrix} 0 & Z_1^T Z_2 \\ Z_2^T Z_1 & 0 \end{pmatrix} \in \{0, 1\}^{m \times m}$ is an adjacency matrix of a bipartite, biregular random graph with uniform distribution over all bipartite, biregular random graphs, the following holds:*

$$\kappa_{m-1,2}^{Diag} = \frac{\lambda_2^{Diag}}{\lambda_{m-1}^{Diag}} \leq \frac{1 + \frac{1}{\sqrt{d_1}} + \frac{1}{\sqrt{d_2}} + \epsilon_m}{1 - \left(\frac{1}{\sqrt{d_1}} + \frac{1}{\sqrt{d_2}}\right) - \epsilon_m} \quad (50)$$

asymptotically almost surely with $\epsilon_m \rightarrow 0$ as $m \rightarrow \infty$, where $d_k = \frac{n}{m_k}$ for $k = 1, 2$.

Proof of Theorem A.1. We have $\lambda_2^{Diag} = 1 + \lambda_2(D^{-1/2} \Lambda D^{-1/2})$ because of (47). Next, (45) gives

$$\lambda_2(D^{-1/2} \Lambda D^{-1/2}) = \lambda_2 \begin{pmatrix} 0 & Z_1^T Z_2 \\ Z_2^T Z_1 & 0 \end{pmatrix} \frac{1}{\sqrt{\sigma^2/\sigma_1^2 + d_1}} \frac{1}{\sqrt{\sigma^2/\sigma_2^2 + d_2}}.$$

Analogously as in the proof of Theorem 4.3, applying Theorem 3.2 of Brito et al. [2022] to $\lambda_2 \begin{pmatrix} 0 & Z_1^T Z_2 \\ Z_2^T Z_1 & 0 \end{pmatrix}$ then shows that

$$\begin{aligned} \lambda_2^{Diag} &\leq 1 + \frac{\sqrt{d_1 - 1} + \sqrt{d_2 - 1}}{\sqrt{\sigma^2/\sigma_1^2 + d_1} \sqrt{\sigma^2/\sigma_2^2 + d_2}} + \epsilon_m \\ &\leq 1 + \frac{1}{\sqrt{d_1}} + \frac{1}{\sqrt{d_2}} + \epsilon_m \end{aligned}$$

asymptotically almost surely with $\epsilon_m \rightarrow 0$ as $m \rightarrow \infty$. Lemma A.1 and analogous arguments give

$$\lambda_{m-1}^{Diag} \geq 1 - \left(\frac{1}{\sqrt{d_1}} + \frac{1}{\sqrt{d_2}}\right) - \epsilon_m.$$

The above two inequalities then result in (50). \square

Proof of Theorem 4.8. Theorem 4.3 shows that

$$\kappa_{m-1,1}^{SSOR} \leq \frac{1}{1 - \frac{4}{d} - \epsilon_m}.$$

Applying the expansion $(1 - x)^{-1} = 1 + x + x^2 + O(x^3)$ with $x = \frac{4}{d} + \epsilon_m$ shows (41). Similarly, Theorem A.1, applying the expansion $(1 - x)^{-1} = 1 + x + x^2 + O(x^3)$ in the denominator of $\frac{1 + \frac{2}{\sqrt{d}} + \epsilon'_m}{1 - \frac{2}{\sqrt{d}} - \epsilon'_m}$, and multiplying by the numerator $1 + \frac{2}{\sqrt{d}} + \epsilon'_m$ give (42). \square

A.3 Proofs of Proposition 3.1, Proposition 3.2, and Proposition 3.3

Proof of Proposition 3.1. By standard results, $\frac{1}{s} \sum_{i=1}^s z_i^{(1)} \odot z_i^{(2)} = \frac{1}{s} \sum_{i=1}^s z_i^{(1)} \odot Z_{po}(\Sigma^{-1} + Z^T W Z)^{-1} Z_{po}^T z_i^{(1)}$ in Algorithm 1 is an unbiased and consistent estimator for $\text{diag}(Z_{po}(\Sigma^{-1} + Z^T W Z)^{-1} Z_{po}^T)$ and $\frac{1}{s} \sum_{i=1}^s z_i^{(1)} \odot z_i^{(3)} = \frac{1}{s} \sum_{i=1}^s z_i^{(1)} \odot Z_{po} P^{-1} Z_{po}^T z_i^{(1)}$ is an unbiased and consistent estimator for $\text{diag}(Z_{po} P^{-1} Z_{po}^T)$. Thus, the claim in Proposition 3.1 follows. \square

Proof of Proposition 3.2. First, observe that $z_i^{(3)} = \Sigma^{-\frac{1}{2}} z_i^{(1)} + Z^T W^{\frac{1}{2}} z_i^{(2)} \sim \mathcal{N}(0, (\Sigma^{-1} + Z^T W Z))$. It follows that $z_i^{(4)} = Z_{po}(\Sigma^{-1} + Z^T W Z)^{-1} z_i^{(3)} \sim \mathcal{N}(0, Z_{po}(\Sigma^{-1} + Z^T W Z)^{-1} Z_{po}^T)$. By standard results, $\frac{1}{s} \sum_{i=1}^s z_i^{(4)} \left(z_i^{(4)}\right)^T$ in Algorithm 2 is an unbiased and consistent estimator for $Z_{po}(\Sigma^{-1} + Z^T W Z)^{-1} Z_{po}^T$, and the claim in Proposition 3.2 thus follows. \square

Proof of Proposition 3.3. First, observe that $z_i^{(3)} = Z \Sigma^{\frac{1}{2}} z_i^{(1)} + W^{-\frac{1}{2}} z_i^{(2)} \sim \mathcal{N}(0, \Psi)$. It follows that $z_i^{(4)} = Z_{po} \Sigma Z^T \Psi^{-1} z_i^{(3)} \sim \mathcal{N}(0, Z_{po} \Sigma Z^T \Psi^{-1} Z \Sigma Z_{po}^T)$. By standard results, $\frac{1}{s} \sum_{i=1}^s z_i^{(4)} \left(z_i^{(4)}\right)^T$ in Algorithm 3 is an unbiased and consistent estimator for $Z_{po} \Sigma Z^T \Psi^{-1} Z \Sigma Z_{po}^T$, and the claim in Proposition 3.3 thus follows. \square

A.4 Derivatives of log-determinants using stochastic trace estimation and variance reduction for SSOR preconditioner

In the following, $c = \widehat{\text{Cov}}(h(z_i), r(z_i)) / \widehat{\text{Var}}(r(z_i))$ is the optimal weight for the variance reduction.

A.4.1 Derivative for variance parameters

Note that $\frac{\partial D}{\partial \theta_k} = \frac{\partial \Sigma^{-1}}{\partial \theta_k} = -\Sigma^{-1} \Sigma^{-1}$.

$$\frac{\partial \log \det(\Sigma^{-1} + Z^T W Z)}{\partial \theta_k} \approx c \underbrace{\frac{\partial \log \det(P_{\text{SSOR}})}{\partial \theta_k}}_{\text{deterministic}} + \frac{\partial \log \det(\Sigma^{-1} + Z^T W Z)}{\partial \theta_k} - c \underbrace{\frac{\partial \log \det(P_{\text{SSOR}})}{\partial \theta_k}}_{\text{stochastic}}$$

$$\begin{aligned} \underbrace{\frac{\partial \log \det(P_{\text{SSOR}})}{\partial \theta_k}}_{\text{deterministic}} &= \frac{\partial (\log \det(L + D) + \log \det(D^{-1}) + \log \det(L + D))}{\partial \theta_k} \\ &= \frac{\partial \log \det(D)}{\partial \theta_k} \\ &= \text{tr} \left(D^{-1} \frac{\partial D}{\partial \theta_k} \right) \end{aligned}$$

$$\begin{aligned} \frac{\partial \log \det(\Sigma^{-1} + Z^T W Z)}{\partial \theta_k} &= \text{tr} \left((\Sigma^{-1} + Z^T W Z)^{-1} \frac{\partial (\Sigma^{-1} + Z^T W Z)}{\partial \theta_k} \right) \\ &= \text{tr} \left((\Sigma^{-1} + Z^T W Z)^{-1} \frac{\partial \Sigma^{-1}}{\partial \theta_k} \right) \\ &= \text{tr} \left(-(\Sigma^{-1} + Z^T W Z)^{-1} \Sigma^{-1} \Sigma^{-1} \right) \\ &\approx \frac{1}{t} \sum_{i=1}^t \underbrace{-((\Sigma^{-1} + Z^T W Z)^{-1} z_i)^T \Sigma^{-1} \Sigma^{-1} P_{\text{SSOR}}^{-1} z_i}_{=: h(z_i)} \end{aligned}$$

$$\begin{aligned} \underbrace{\frac{\partial \log \det(P_{\text{SSOR}})}{\partial \theta_k}}_{\text{stochastic}} &= \text{tr} \left(P_{\text{SSOR}}^{-1} \frac{\partial P_{\text{SSOR}}}{\partial \theta_k} \right) \\ &= \text{tr} \left(P_{\text{SSOR}}^{-1} \frac{\partial (L + D) D^{-1} (L + D)^T}{\partial \theta_k} \right) \\ &= \text{tr} \left(P_{\text{SSOR}}^{-1} \left(2 \frac{\partial D}{\partial \theta_k} D^{-1} (L + D)^T - (L + D) D^{-1} \frac{\partial D}{\partial \theta_k} D^{-1} (L + D)^T \right) \right) \\ &\approx \frac{1}{t} \sum_{i=1}^t \underbrace{(P_{\text{SSOR}}^{-1} z_i)^T \left(2 \frac{\partial D}{\partial \theta_k} D^{-1} (L + D)^T - (L + D) D^{-1} \frac{\partial D}{\partial \theta_k} D^{-1} (L + D)^T \right) P_{\text{SSOR}}^{-1} z_i}_{=: r(z_i)} \end{aligned}$$

A.4.2 Further derivatives for Laplace approximations

For efficient calculations of the derivatives of log-determinants with STE, note that $\frac{\partial \log \det(\Sigma^{-1} + Z^T W Z)}{\partial F_i} = \frac{\partial \log \det(\Sigma^{-1} + Z^T W Z)}{\partial \mu_i^*}$ and $\frac{\partial \log \det(\Sigma^{-1} + Z^T W Z)}{\partial b_j^*} = \left(\frac{\partial \log \det(\Sigma^{-1} + Z^T W Z)}{\partial \mu^*} \right)^T \frac{\partial \mu^*}{\partial b_j^*} = \left(\frac{\partial \log \det(\Sigma^{-1} + Z^T W Z)}{\partial \mu^*} \right)^T Z_j$.

Therefore, we present in the following calculations for $\frac{\partial \log \det(\Sigma^{-1} + Z^T W Z)}{\partial \mu_i^*}$, and $\frac{\partial \log \det(\Sigma^{-1} + Z^T W Z)}{\partial \xi_l}$ is obtained by replacing $\frac{\partial W}{\partial \mu_i^*} = \text{diag}(-\frac{\partial^3 \log p(y_i | \mu_i^*, \xi)}{\partial \mu_i^{*3}})$ with $\frac{\partial W}{\partial \xi_l} = \text{diag}(-\frac{\partial^3 \log p(y_i | \mu_i^*, \xi)}{\partial \mu_i^{*2} \partial \xi_l})$. Further, $\frac{\partial D}{\partial \mu_i^*}$ is a diagonal matrix with diagonal entries $\left(\frac{\partial D}{\partial \mu_i^*} \right)_{ii} = \left(Z^T \frac{\partial W}{\partial \mu_i^*} Z \right)_{ii}$, and $\frac{\partial (L+D)}{\partial \mu_i^*}$ is a lower-triangular matrix with entries $\left(\frac{\partial (L+D)}{\partial \mu_i^*} \right)_{ij} = \mathbf{1}_{\{i > j\}} \left(Z^T \frac{\partial W}{\partial \mu_i^*} Z \right)_{ij}$.

$$\begin{aligned}
\frac{\partial \log \det(\Sigma^{-1} + Z^T W Z)}{\partial \mu_i^*} &\approx c \underbrace{\frac{\partial \log \det(P_{\text{SSOR}})}{\partial \mu_i^*}}_{\text{deterministic}} + \frac{\partial \log \det(\Sigma^{-1} + Z^T W Z)}{\partial \mu_i^*} - c \underbrace{\frac{\partial \log \det(P_{\text{SSOR}})}{\partial \mu_i^*}}_{\text{stochastic}} \\
\frac{\partial \log \det(P_{\text{SSOR}})}{\partial \mu_i^*} &= \frac{\partial (\log \det(L + D) + \log \det(D^{-1}) + \log \det(L + D))}{\partial \mu_i^*} \\
&= \frac{\partial \log \det(D)}{\partial \mu_i^*} \\
&= \text{tr} \left(D^{-1} \frac{\partial D}{\partial \mu_i^*} \right) \\
\frac{\partial \log \det(\Sigma^{-1} + Z^T W Z)}{\partial \mu_i^*} &= \text{tr} \left((\Sigma^{-1} + Z^T W Z)^{-1} \frac{\partial (\Sigma^{-1} + Z^T W Z)}{\partial \mu_i^*} \right) \\
&= \text{tr} \left((\Sigma^{-1} + Z^T W Z)^{-1} Z^T \frac{\partial W}{\partial \mu_i^*} Z \right) \\
&\approx \frac{1}{t} \sum_{i=1}^t \underbrace{((\Sigma^{-1} + Z^T W Z)^{-1} z_i)^T Z^T \frac{\partial W}{\partial \mu_i^*} Z P_{\text{SSOR}}^{-1} z_i}_{=: h(z_i)} \\
\frac{\partial \log \det(P_{\text{SSOR}})}{\partial \mu_i^*} &= \text{tr} \left(P_{\text{SSOR}}^{-1} \frac{\partial P_{\text{SSOR}}}{\partial \mu_i^*} \right) \\
&= \text{tr} \left(P_{\text{SSOR}}^{-1} \frac{\partial (L + D) D^{-1} (L + D)^T}{\partial \mu_i^*} \right) \\
&= \text{tr} \left(P_{\text{SSOR}}^{-1} \left(2 \frac{\partial (L + D)}{\partial \mu_i^*} D^{-1} (L + D)^T - (L + D) D^{-1} \frac{\partial D}{\partial \mu_i^*} D^{-1} (L + D)^T \right) \right) \\
&\approx \frac{1}{t} \sum_{i=1}^t \underbrace{(P_{\text{SSOR}}^{-1} z_i)^T \left(2 \frac{\partial (L + D)}{\partial \mu_i^*} D^{-1} (L + D)^T - (L + D) D^{-1} \frac{\partial D}{\partial \mu_i^*} D^{-1} (L + D)^T \right) P_{\text{SSOR}}^{-1} z_i}_{=: r(z_i)}
\end{aligned}$$

A.5 Alternative stochastic trace estimation for Fisher information

For $1 \leq k, l \leq K$ and $z_i \sim \mathcal{N}(0, P)$, the trace terms of the Fisher information in (7) can alternatively be computed with STE as follows:

$$\begin{aligned}
&\text{tr} \left(\Psi^{-1} \frac{\partial \Psi}{\partial \theta_k} \Psi^{-1} \frac{\partial \Psi}{\partial \theta_l} \right) \\
&= \text{tr} \left((W - WZ(\Sigma^{-1} + Z^T W Z)^{-1} Z^T W) Z_k Z_k^T \right. \\
&\quad \left. (W - WZ(\Sigma^{-1} + Z^T W Z)^{-1} Z^T W) Z_l Z_l^T \right) \\
&= \text{tr} (W Z_k Z_k^T W Z_l Z_l^T) \\
&\quad - 2 \text{tr} ((\Sigma^{-1} + Z^T W Z)^{-1} Z^T W Z_k Z_k^T W Z_l Z_l^T ZW) \\
&\quad + \text{tr} ((\Sigma^{-1} + Z^T W Z)^{-1} Z^T W Z_k Z_k^T W Z(\Sigma^{-1} + Z^T W Z)^{-1} Z^T W Z_l Z_l^T ZW) \\
&\approx \text{tr} (W Z_k Z_k^T W Z_l Z_l^T) \\
&\quad - 2 \frac{1}{t} \sum_{i=1}^t ((\Sigma^{-1} + Z^T W Z)^{-1} z_i)^T Z^T W Z_k Z_k^T W Z_l Z_l^T ZW P^{-1} z_i \\
&\quad + \frac{1}{t} \sum_{i=1}^t ((\Sigma^{-1} + Z^T W Z)^{-1} z_i)^T Z^T W Z_k Z_k^T W Z(\Sigma^{-1} + Z^T W Z)^{-1} Z^T W Z_l Z_l^T ZW P^{-1} z_i.
\end{aligned} \tag{51}$$

A.6 Preconditioned conjugate gradient algorithm

Algorithm 4 Preconditioned conjugate gradient algorithm with Lanczos tridiagonal matrix

Input: Matrix A , preconditioner matrix P , vector b

Output: $u_{l+1} \approx A^{-1}b$, tridiagonal matrix \tilde{T}

```

1: early-stopping  $\leftarrow$  false
2:  $\alpha_0 \leftarrow 1$ 
3:  $\beta_0 \leftarrow 0$ 
4:  $u_0 \leftarrow 0$ 
5:  $r_0 \leftarrow b - Au_0$ 
6:  $z_0 \leftarrow P^{-1}r_0$ 
7:  $h_0 \leftarrow z_0$ 
8: for  $l \leftarrow 0$  to  $L$  do
9:    $v_l \leftarrow Ah_l$ 
10:   $\alpha_{l+1} \leftarrow \frac{r_l^T z_l}{h_l^T v_l}$ 
11:   $u_{l+1} \leftarrow u_l + \alpha_{l+1} h_l$ 
12:   $r_{l+1} \leftarrow r_l - \alpha_{l+1} v_l$ 
13:  if  $\|r_{l+1}\|_2 < \text{tolerance}$  then
14:    early-stopping  $\leftarrow$  true
15:  end if
16:   $z_{l+1} \leftarrow P^{-1}r_{l+1}$ 
17:   $\beta_{l+1} \leftarrow \frac{r_{l+1}^T z_{l+1}}{r_l^T z_l}$ 
18:   $h_{l+1} \leftarrow z_{l+1} + \beta_{l+1} h_l$ 
19:   $\tilde{T}_{l+1,l+1} \leftarrow \frac{1}{\alpha_{l+1}} + \frac{\beta_l}{\alpha_l}$ 
20:  if  $l > 0$  then
21:     $\tilde{T}_{l,l+1}, \tilde{T}_{l+1,l} \leftarrow \frac{\sqrt{\beta_l}}{\alpha_l}$ 
22:  end if
23:  if early-stopping then
24:    return  $u_{l+1}, \tilde{T}$ 
25:  end if
26: end for

```

A.7 Zero fill-in incomplete Cholesky factorization

Algorithm 5 Zero fill-in incomplete Cholesky algorithm

Input: Matrix $A \in \mathbb{R}^{m \times m}$, matrix $S \in \mathbb{R}^{m \times m}$ with sparsity pattern

Output: Sparse lower triangular matrix L with $A \approx LL^T$

```

1: for  $i \leftarrow 1$  to  $m$  do
2:   for  $j \leftarrow 1$  to  $m$  do
3:     if  $(i, j) \in S$  and  $i \geq j$  then
4:        $s \leftarrow L_i \cdot L_j^T$ 
5:       if  $i == j$  then
6:          $L_{ii} \leftarrow \sqrt{A_{ii} - s}$ 
7:       else
8:          $L_{ij} \leftarrow \frac{A_{ij} - s}{L_{jj}}$ 
9:       end if
10:    end if
11:  end for
12: end for

```

A.8 Additional results for preconditioner comparison

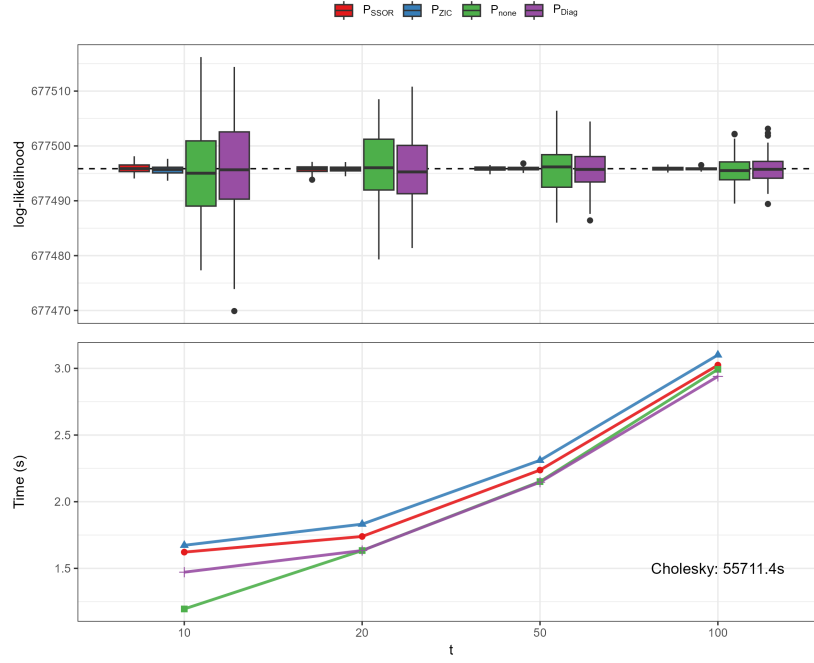


Figure 9: Negative log-marginal likelihood and wall-clock time in seconds for different preconditioners and numbers of random vectors t when the response variable follows a Bernoulli likelihood with a logit link function. The dashed line represents the result for the Cholesky decomposition.

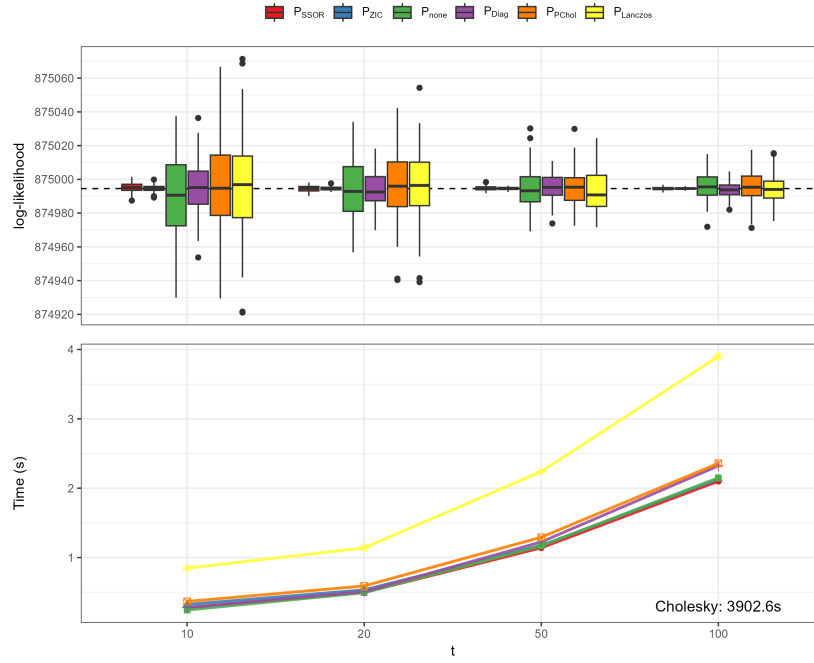


Figure 10: Negative log-marginal likelihood and wall-clock time in seconds for different preconditioners and numbers of random vectors t when $m_2 = \frac{m_1}{2}$, $m = m_1 + m_2 = 99'999$, $n = 10m$, and the response variable follows a Gaussian likelihood. The dashed line represents the result for the Cholesky decomposition.

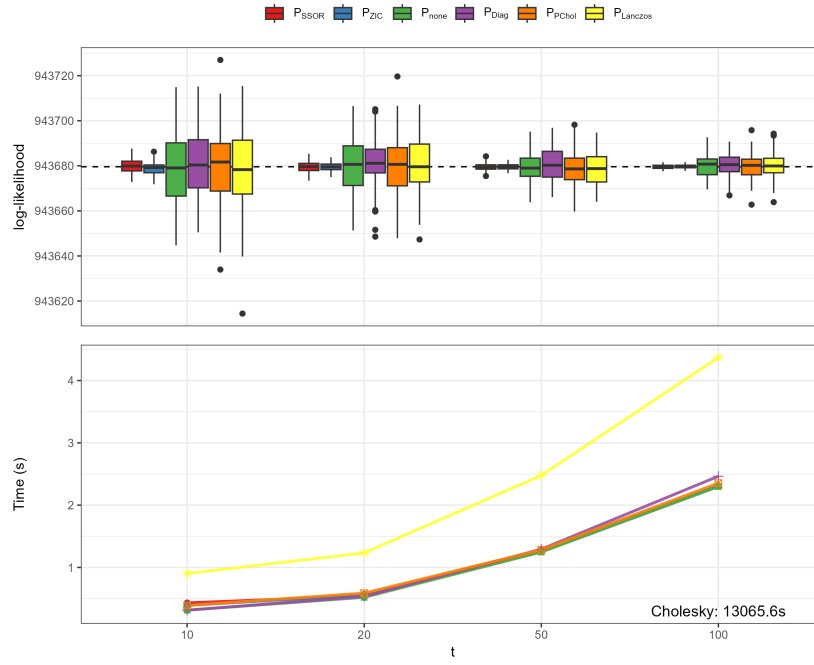


Figure 11: Negative log-marginal likelihood and wall-clock time in seconds for different preconditioners and numbers of random vectors t when $\sigma^2 = 0.25$, $\sigma_1^2 = \sigma_2^2 = 1$, and the response variable follows a Gaussian likelihood. The dashed line represents the result for the Cholesky decomposition.

A.9 Additional results for parameter estimation and prediction in simulated experiments

	Krylov (GPBoost)	Cholesky (GPBoost)	lme4	glmmTMB
RMSE σ^2	1.75×10^{-3}	1.75×10^{-3}	1.73×10^{-3}	1.73×10^{-3}
Bias σ^2	1.24×10^{-4}	1.26×10^{-4}	1.23×10^{-4}	1.23×10^{-4}
RMSE σ_1^2	8.97×10^{-3}	8.96×10^{-3}	8.83×10^{-3}	8.83×10^{-3}
Bias σ_1^2	-5.96×10^{-4}	-6.15×10^{-4}	-5.57×10^{-4}	-5.57×10^{-4}
RMSE σ_2^2	8.34×10^{-3}	8.35×10^{-3}	8.13×10^{-3}	8.13×10^{-3}
Bias σ_2^2	1.79×10^{-4}	1.56×10^{-4}	1.53×10^{-4}	1.54×10^{-4}
RMSE β_0	1.46×10^{-2}	1.46×10^{-2}	1.46×10^{-2}	1.46×10^{-2}
Bias β_0	1.36×10^{-3}	1.36×10^{-3}	1.36×10^{-3}	1.36×10^{-3}
RMSE β_1	1.17×10^{-2}	1.17×10^{-2}	1.17×10^{-2}	1.17×10^{-2}
Bias β_1	-2.06×10^{-4}	-2.06×10^{-4}	-2.06×10^{-4}	-2.06×10^{-4}
RMSE β_2	1.08×10^{-2}	1.08×10^{-2}	1.08×10^{-2}	1.08×10^{-2}
Bias β_2	-4.41×10^{-4}	-4.41×10^{-4}	-4.41×10^{-4}	-4.41×10^{-4}
RMSE β_3	1.25×10^{-2}	1.25×10^{-2}	1.25×10^{-2}	1.25×10^{-2}
Bias β_3	-1.14×10^{-3}	-1.14×10^{-3}	-1.14×10^{-3}	-1.14×10^{-3}
RMSE β_4	1.31×10^{-2}	1.31×10^{-2}	1.31×10^{-2}	1.31×10^{-2}
Bias β_4	1.28×10^{-3}	1.28×10^{-3}	1.28×10^{-3}	1.28×10^{-3}
RMSE β_5	1.06×10^{-2}	1.06×10^{-2}	1.06×10^{-2}	1.06×10^{-2}
Bias β_5	3.21×10^{-4}	3.21×10^{-4}	3.21×10^{-4}	3.21×10^{-4}

Table 2: Root mean squared error (RMSE) and bias of the variance and coefficient estimates for Gaussian likelihoods.

	Krylov (GPBoost)	Cholesky (GPBoost)	glmmTMB
RMSE σ_1^2	2.01×10^{-2}	2.01×10^{-2}	2.05×10^{-2}
Bias σ_1^2	-1.15×10^{-2}	-1.15×10^{-2}	-1.13×10^{-2}
RMSE σ_2^2	2.15×10^{-2}	2.15×10^{-2}	2.20×10^{-2}
Bias σ_2^2	-1.36×10^{-2}	-1.36×10^{-2}	-1.36×10^{-2}
RMSE β_0	1.73×10^{-2}	1.73×10^{-2}	1.73×10^{-2}
Bias β_0	-3.68×10^{-4}	-3.67×10^{-4}	-4.76×10^{-4}
RMSE β_1	5.18×10^{-2}	5.18×10^{-2}	5.10×10^{-2}
Bias β_1	1.33×10^{-3}	1.34×10^{-3}	7.09×10^{-4}
RMSE β_2	5.33×10^{-2}	5.33×10^{-2}	5.19×10^{-2}
Bias β_2	-6.51×10^{-3}	-6.53×10^{-3}	-5.87×10^{-3}
RMSE β_3	5.10×10^{-2}	5.09×10^{-2}	5.05×10^{-2}
Bias β_3	6.00×10^{-4}	5.82×10^{-4}	1.86×10^{-4}
RMSE β_4	5.25×10^{-2}	5.25×10^{-2}	5.24×10^{-2}
Bias β_4	-1.24×10^{-3}	-1.23×10^{-3}	-1.30×10^{-3}
RMSE β_5	5.18×10^{-2}	5.18×10^{-2}	4.99×10^{-2}
Bias β_5	-6.36×10^{-3}	-6.36×10^{-3}	-5.61×10^{-3}

Table 3: Root mean squared error (RMSE) and bias of the variance and coefficient estimates for Bernoulli likelihoods.

	Krylov (GPBoost)	Cholesky (GPBoost)	lme4	glmmTMB
RMSE	1.62×10^{-1}	1.62×10^{-1}	1.62×10^{-1}	1.62×10^{-1}
sd(RMSE)	2.32×10^{-4}	2.32×10^{-4}	2.32×10^{-4}	2.32×10^{-4}
\overline{LS}	-4.01×10^{-1}	-4.01×10^{-1}		
sd(\overline{LS})	1.40×10^{-3}	1.40×10^{-3}		

Table 4: Average root mean squared error (RMSE) for predictive means and average log score (LS) for probabilistic predictions with corresponding standard errors for Gaussian likelihoods.

	Krylov (GPBoost)	Cholesky (GPBoost)	glmmTMB
RMSE	5.00×10^{-1}	5.00×10^{-1}	5.00×10^{-1}
sd(RMSE)	5.37×10^{-4}	5.37×10^{-4}	5.37×10^{-4}
\overline{LS}	7.26×10^{-1}	7.26×10^{-1}	
sd(\overline{LS})	1.12×10^{-3}	1.12×10^{-3}	

Table 5: Average root mean squared error (RMSE) for predictive means and average log score (LS) for probabilistic predictions with corresponding standard errors for Bernoulli likelihoods.

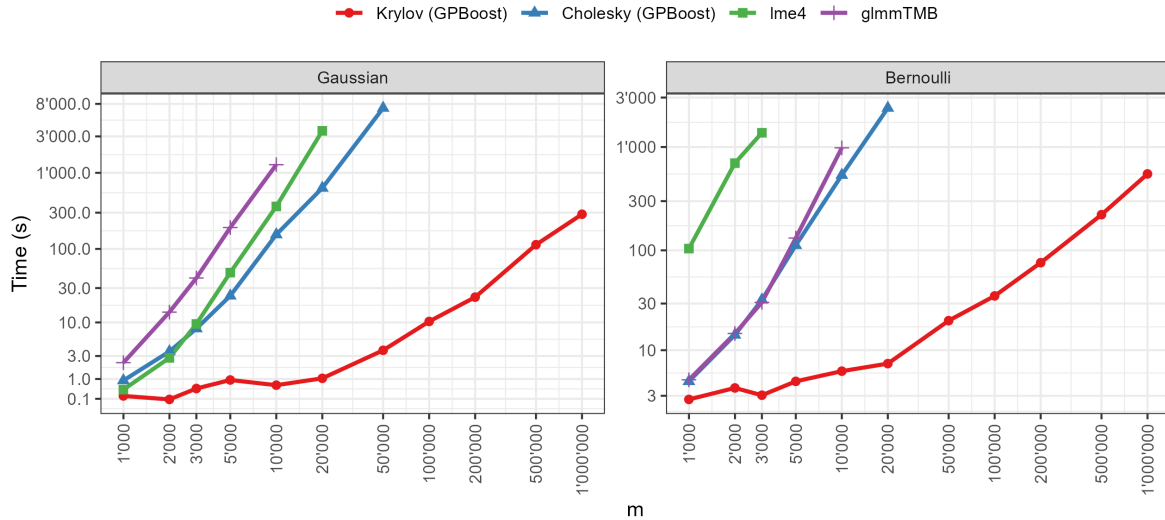


Figure 12: Average wall clock times (s) for parameter estimation and different m with $m_2 = \frac{m_1}{2}$. The dimensions of the random effects m are chosen so that they are divisible by three and correspond as closely as possible to those in Figure 6. Simulated data follows either a Gaussian or a Bernoulli likelihood.

A.10 Additional results for the real-world applications

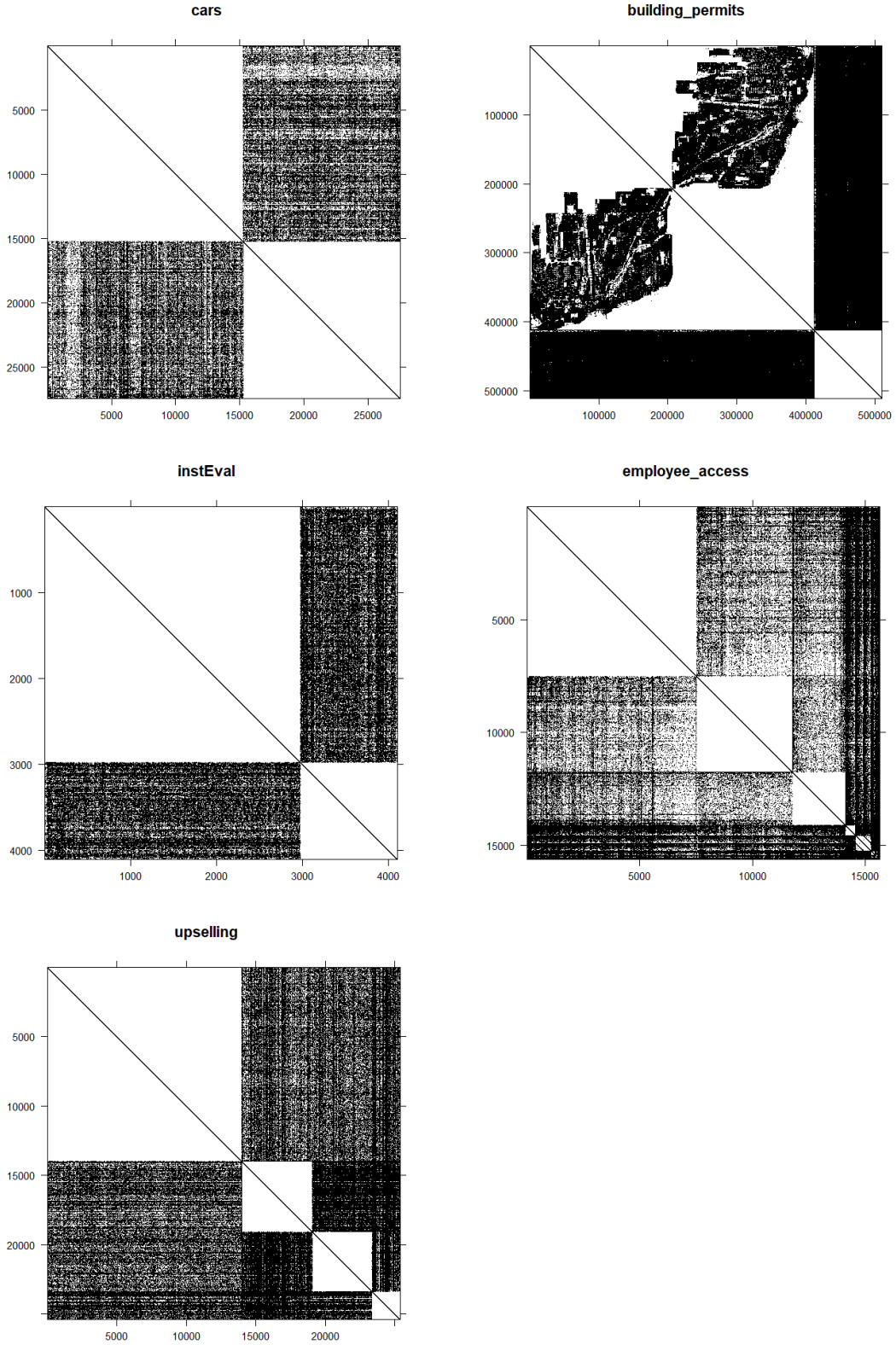


Figure 13: Non-zero entries of the matrix $Z^T Z$ for the real-world data sets.

data set	method	Time (s)	nll_optimum
cars	Cholesky (GPBoost)	104.3	27518.0
	Krylov (GPBoost)	7.7	27517.1
	glmmTMB	1152.2	27518.1
	lme4	62.3	27518.0
building_permits	Cholesky (GPBoost)	5647.5	867567.7
	Krylov (GPBoost)	97.4	867566.5
	glmmTMB	3763.2	867567.8
	lme4	600.0	867567.3
instEval	Cholesky (GPBoost)	9.4	118764.0
	Krylov (GPBoost)	0.5	118763.5
	glmmTMB	76.1	118764.0
	lme4	11.5	118764.0
employee_access	Cholesky (GPBoost)	628.0	5494.4
	Krylov (GPBoost)	80.5	5492.3
	glmmTMB	287.9	5494.4
	lme4	8362.9	5504.5
upselling	Cholesky (GPBoost)	1747.8	11488.5
	Krylov (GPBoost)	41.1	11488.4

Table 6: Time for parameter estimation and negative log-marginal likelihood at the optimum for different real-world data sets and models.

data set	method	σ^2	σ_1^2	σ_2^2	σ_3^2
cars	Cholesky (GPBoost)	5.24×10^{-2}	3.28×10^{-1}	2.04×10^{-1}	
	Krylov (GPBoost)	5.24×10^{-2}	3.28×10^{-1}	2.04×10^{-1}	
	glmmTMB	5.24×10^{-2}	3.28×10^{-1}	2.04×10^{-1}	
	lme4	5.24×10^{-2}	3.28×10^{-1}	2.04×10^{-1}	
building_permits	Cholesky (GPBoost)	1.31×10^0	9.10×10^{-1}	3.98×10^{-2}	3.97×10^{-2}
	Krylov (GPBoost)	1.31×10^0	9.09×10^{-1}	3.98×10^{-2}	3.96×10^{-2}
	glmmTMB	1.31×10^0	9.10×10^{-1}	3.69×10^{-2}	4.25×10^{-2}
	lme4	1.31×10^0	9.10×10^{-1}	7.93×10^{-2}	1.08×10^{-4}
instEval	Cholesky (GPBoost)	1.38×10^0	1.07×10^{-1}	2.57×10^{-1}	
	Krylov (GPBoost)	1.38×10^0	1.07×10^{-1}	2.57×10^{-1}	
	glmmTMB	1.38×10^0	1.07×10^{-1}	2.57×10^{-1}	
	lme4	1.38×10^0	1.07×10^{-1}	2.57×10^{-1}	
employee_access	Cholesky (GPBoost)		1.52×10^0	5.78×10^0	9.48×10^{-6}
	Krylov (GPBoost)		1.52×10^0	5.79×10^0	1.17×10^{-5}
	glmmTMB		1.52×10^0	5.78×10^0	3.14×10^{-10}
	lme4		1.60×10^0	6.06×10^0	0.00×10^0
upselling	Cholesky (GPBoost)		3.56×10^{-1}	2.59×10^{-1}	9.86×10^{-3}
	Krylov (GPBoost)		3.58×10^{-1}	2.58×10^{-1}	9.58×10^{-3}

Table 7: Estimates for σ^2 , σ_1^2 , σ_2^2 , and σ_3^2 for different real-world data sets and models. For reasons of space, we do not report estimates for other variance parameters.

data set	method	β_0	β_1	β_2	β_3
cars	Cholesky (GPBoost)	1.02×10^1	3.50×10^{-1}	-1.77×10^{-1}	-2.64×10^{-3}
	Krylov (GPBoost)	1.02×10^1	3.50×10^{-1}	-1.77×10^{-1}	-2.64×10^{-3}
	glmmTMB	1.02×10^1	3.50×10^{-1}	-1.77×10^{-1}	-2.63×10^{-3}
	lme4	1.02×10^1	3.50×10^{-1}	-1.77×10^{-1}	-2.64×10^{-3}
building_permits	Cholesky (GPBoost)	3.62×10^0	5.44×10^{-4}	-1.36×10^{-5}	2.01×10^{-3}
	Krylov (GPBoost)	3.62×10^0	5.44×10^{-4}	-1.36×10^{-5}	2.00×10^{-3}
	glmmTMB	3.62×10^0	5.44×10^{-4}	-1.36×10^{-5}	2.02×10^{-3}
	lme4	3.62×10^0	5.44×10^{-4}	-1.36×10^{-5}	2.01×10^{-3}
instEval	Cholesky (GPBoost)	3.31×10^0	5.21×10^{-2}	7.23×10^{-2}	1.37×10^{-1}
	Krylov (GPBoost)	3.31×10^0	5.21×10^{-2}	7.23×10^{-2}	1.37×10^{-1}
	glmmTMB	3.31×10^0	5.21×10^{-2}	7.23×10^{-2}	1.37×10^{-1}
	lme4	3.31×10^0	5.21×10^{-2}	7.23×10^{-2}	1.37×10^{-1}
employee_access	Cholesky (GPBoost)	7.21×10^0			
	Krylov (GPBoost)	7.16×10^0			
	glmmTMB	7.19×10^0			
	lme4	6.92×10^0			
upselling	Cholesky (GPBoost)	-1.74×10^0	2.32×10^{-5}	9.42×10^{-3}	3.86×10^{-6}
	Krylov (GPBoost)	-1.74×10^0	2.32×10^{-5}	9.48×10^{-3}	3.94×10^{-6}

Table 8: Estimates for β_0 , β_1 , β_2 , and β_3 for different real-world data sets and models. For reasons of space, we do not report estimates for other coefficients.